



Early View

Original article

Pharmacometabolic response to pirfenidone in pulmonary fibrosis detected by MALDI-FTICR-MSI

Na Sun, Isis E. Fernandez, Mian Wei, Michael Witting, Michaela Aichler, Annette Feuchtinger, Gerald Burgstaller, Stijn E. Verleden, Philippe Schmitt-Kopplin, Oliver Eickelberg, Axel Walch

Please cite this article as: Sun N, Fernandez IE, Wei M, *et al.* Pharmacometabolic response to pirfenidone in pulmonary fibrosis detected by MALDI-FTICR-MSI. *Eur Respir J* 2018; in press (<https://doi.org/10.1183/13993003.02314-2017>).

This manuscript has recently been accepted for publication in the *European Respiratory Journal*. It is published here in its accepted form prior to copyediting and typesetting by our production team. After these production processes are complete and the authors have approved the resulting proofs, the article will move to the latest issue of the ERJ online.

Copyright ©ERS 2018

**Pharmacometabolic response to pirfenidone in pulmonary fibrosis detected by
MALDI-FTICR-MSI**

Na Sun¹⁺, Isis E. Fernandez²⁺, Mian Wei¹, Michael Witting³, Michaela Aichler¹, Annette Feuchtinger¹, Gerald Burgstaller², Stijn E. Verleden⁴, Philippe Schmitt-Kopplin³, Oliver Eickelberg^{2,5*}, Axel Walch^{1*}

¹Research Unit Analytical Pathology, Helmholtz Zentrum München, German Research Centre for Environmental Health (GmbH), Neuherberg, Germany

²Comprehensive Pneumology Centre, Helmholtz Zentrum München, Ludwig Maximilian University München. Member of the German Centre for Lung Research (DZL), München, Germany

³Research Unit Analytical BioGeoChemistry, Helmholtz Zentrum München, German Research Centre for Environmental Health (GmbH), Neuherberg, Germany

⁴Lab of Pneumology, department of Chronic Diseases, Metabolism and Aging, KU Leuven, Leuven Belgium

⁵Division of Respiratory Sciences and Critical Care Medicine, Department of Medicine, University of Colorado, Denver, CO, USA.

*To whom correspondence should be addressed: Oliver Eickelberg: oliver.eickelberg@ucdenver.edu, Axel Walch: axel.walch@helmholtz-muenchen.de.

+*These authors contributed equally.

(<http://erj.ersjournals.com/authors/instructions>)

Abstract

Idiopathic pulmonary fibrosis (IPF) is a fatal condition that reduces life expectancy and shows a limited response to available therapies. Pirfenidone has been approved for treatment of IPF, but little is known about the distinct metabolic changes that occur in the lung upon pirfenidone administration. Here, we performed a proof-of-concept study using high-resolution quantitative Matrix-Assisted Laser Desorption/Ionization Fourier-Transform Ion Cyclotron Resonance-Mass Spectrometry Imaging (MALDI-FTICR-MSI) to simultaneously detect, visualize, and quantify *in situ* endogenous and exogenous metabolites in lungs of mice subjected to experimental fibrosis and human patients with IPF and to assess the effect of pirfenidone treatment on metabolite levels. Metabolic pathway analysis and endogenous metabolite quantification revealed that pirfenidone treatment restores redox imbalance and glycolysis in IPF tissues, and down-regulates ascorbate and aldarate metabolism, thereby likely contributing to *in situ* modulation of collagen processing. As such, we detected specific alterations in metabolite pathways in fibrosis, and importantly, metabolic recalibration following pirfenidone treatment. Together, these results highlight the suitability of high-resolution MALDI-FTICR-MSI for deciphering the therapeutic effects of pirfenidone and provide a preliminary analysis of the metabolic changes that occur during pirfenidone treatment *in vivo*. These data may therefore contribute to improvement of currently available therapies for IPF.

Introduction

Idiopathic pulmonary fibrosis (IPF) is a chronic progressive and diffuse parenchymal lung disease that leads to loss of organ function. IPF is characterized by replacement of lung parenchyma with fibrotic tissue, aberrant fibroblast-myofibroblast activation, epithelial hyperplasia and injury, and immune dysregulation (1). IPF is considered to be an incurable lethal disease, with median survival ranging from 2-3 years, worse than many cancers.

Pirfenidone (5-methyl-1-phenyl-2-(1H)-pyridone) is an orally active pyridine molecule that exhibits anti-fibrotic and anti-inflammatory activities (2, 3). It is approved for IPF treatment worldwide, including the European Union and the United States, where it is one of two drugs approved for use in IPF patients (4). Although pirfenidone is a first-line drug for IPF treatment (5), its precise mechanism of action has not been elucidated to-date (6). In an effort to better guide treatment of IPF, we here seek to better understand the detailed mechanism of pirfenidone activity.

In situ metabolite imaging is a high-throughput, non-targeted metabolomic technique that has been refined by ultra-sensitive and high-resolution quantitative Matrix-Assisted Laser Desorption/Ionization-Mass Spectrometry Imaging (MALDI-MSI), with Fourier-Transform Ion Cyclotron Resonance (FTICR) and Orbitrap (7-11). High mass-resolution MALDI-MSI enables simultaneous mapping of spatial distribution for a wide range of low-molecular-weight metabolites, including central metabolic pathway metabolites, redox-related metabolites, nucleotide derivatives, lipids, and amino acids, directly within morphologically intact tissue sections. MALDI-MSI mass spectra are acquired by measuring spots in a predefined raster across a tissue section, resulting in a two-dimensional distribution map for each measured molecule (12, 13). Therefore, MALDI-MSI allows acquisition of cellular expression profiles, while preserving cellular and molecular integrity. This technology excels at imaging spatial organization of molecules within histological features (14) and can characterize molecular interaction networks of several functionally distinct pathways (15).

Metabolic changes in IPF pathogenesis, particularly patient-specific responses to drug treatment, remain poorly understood. Recent liquid-based metabolomic studies of IPF have reported several disrupted pathways, including sphingolipid metabolism, glycolysis, the tricarboxylic acid (TCA) cycle, arginine metabolism, adenosine triphosphate, glutathione

biosynthesis, and ornithine aminotransferase (16, 17). We recently reported that high-resolution MALDI-FTICR-MSI can accurately detect distribution and pharmacokinetics of pirfenidone and pirfenidone-related metabolites, 5-hydroxymethyl pirfenidone and 5-carboxy pirfenidone, in healthy mouse tissues. Notably, in that study, we did not observe consistent effects of pirfenidone, or its metabolites, on known metabolic pathways (18).

Here, to explore endogenous metabolite dynamics upon pirfenidone treatment in fibrotic lungs, we used high-resolution MALDI-FTICR-MSI and performed the first tissue-based *in situ* metabolite imaging on treatment-naïve and pirfenidone-treated IPF patients, as well as an experimental mouse model of this disease. We provide a proof-of-concept for the use of this technique to assess dynamic metabolic changes occurring in IPF and in patients treated with pirfenidone.

Materials and methods

Experimental mouse model of pulmonary fibrosis

All animal experiments utilised 8- to 10-week-old female C57BL/6N mice (Charles River Laboratories) and were performed in accordance with recommendations in the Guide for the Care and Use of Laboratory Animals of the National Institutes of Health (NIH). Pulmonary fibrosis in mice was established as described (ethical approval number: TVA21-12) (19). Briefly, bleomycin (3 U/kg) or phosphate-buffered saline (PBS) was applied intratracheally as a single dose. From day 7-14 post-treatment, a subset of both bleomycin-treated and control animals was administered oral pirfenidone daily (Selleckchem, Houston, TX, USA); see supplemental material. All animals (PBS=3, PBS+pirfenidone=3, bleomycin=3, bleomycin+pirfenidone=3) were sacrificed on day 14.

Human lung samples

This study was approved by the hospital ethics and university biosafety committees in Leuven, Belgium. Explanted lung tissue from IPF patients that were either untreated or under pirfenidone treatment, or donor controls, were collected at KU Leuven, under ethical approval number: ML6385. Protocols for processing and sampling lung specimens have been described in detail (20). Briefly, each lung was inflated with air to a transpulmonary pressure of 30 cmH₂O, then deflated to 10 cmH₂O while freezing in liquid nitrogen vapour;

frozen samples were stored at -80°C . Lungs (IPF=4, pirfenidone-treated IPF=3, donor=4) were cut into 2-cm-thick slices; cores with a diameter of 1.4 cm were excised and processed as described (21).

Immunofluorescence in frozen tissue

Slides containing sections of frozen lung were fixed by immersion in 2% paraformaldehyde (PFA) for 5 min, then dipped in distilled water, followed by a short wash in tris-buffered saline with Tween 20 (TBS-T). These were blocked by immersion in 3% hydrogen peroxide:distilled water solution (10 min), followed by a 3% bovine serum albumin (BSA):TBS-T buffer solution (20 min), to prevent non-specific binding. Slides were stained with Collagen Type I (COL1) Antibody (Rockland Immunochemicals Inc., 600-401-103-0.1), diluted (1:250) with antibody diluent (Zytomed Systems, Berlin, Germany). COL1 antibody staining was performed in a wet chamber at 4°C , overnight. Slides were then rinsed three times with TBS-T, and a 1:250 dilution of secondary antibody (Alexa Fluor 568 donkey anti-rabbit) was applied, followed by incubation at room temperature (1 h) in the dark. Slides were counterstained with 4',6-diamidino-2-phenylindole (DAPI, 1:2500; Sigma-Aldrich; St Louis, MO, USA) for 1 min and then rinsed three times with TBS-T buffer. They were then covered with Fluorescence Mounting Medium (Dako, Hamburg, Germany) and scanned using an AxioScan.Z1 digital slide scanner (Zeiss, Goettingen, Germany), equipped with a 20x magnification objective.

MALDI-FT-ICR-MSI

For the endogenous metabolomics study, MALDI-FT-ICR-MSI (solariX 7T, Bruker Daltonics) measurements were performed in the mass range of m/z 50–1,000 in negative ion mode at a frequency of 500 Hz, using 50 laser shots and a spatial resolution of 70 μm .

For the drug imaging study of pirfenidone and its related metabolites, 5-hydroxymethyl pirfenidone and 5-carboxy pirfenidone, MALDI-FTICR-MSI (solariX 7T, Bruker Daltonics) was performed in continuous accumulation of selected ions (CASI) mode. Mass-selective quadrupole was set to 186.1 m/z , with a window of 130 m/z . Mass spectra were acquired with a 70 μm spatial resolution in positive mode, using 100 laser shots, at a frequency of 1 kHz.

Metabolite identification by LC-MS and tissue MS/MS and pathway analysis

Targeted metabolite identification by liquid chromatography-mass spectrometry (LC-MS) was performed as described (22). Complementary experiments for metabolite identification using tissue tandem mass spectrometry (MS/MS) analysis was performed with MALDI-FTICR-MSI (solariX 7T, Bruker Daltonics) using CASI mode, which allows target ion selection in quadrupole and fragmented using collision-induced dissociation. Metabolites were identified or estimated by comparing MS/MS spectra with standard compounds or by matching accurate mass with databases, as described (15), (22), (23) (METLIN, <http://metlin.scripps.edu/>; MassTRIX, <http://masstrix3.helmholtz-muenchen.de/masstrix3/>; METASPACE, <http://annotate.metaspaces2020.eu/> (24); and Human Metabolome Database, <http://www.hmdb.ca/> (25). These databases were used in conjunction with MetaboAnalyst (<http://www.metaboanalyst.ca/>) (26) and KEGG (<http://www.genome.jp/kegg/>) for pathway analysis. Details of MALDI-MSI tissue preparation, data processing and statistical analysis, relative quantification of endogenous metabolites, and metabolite identification by LC-MS are provided in the online supplementary data.

Results

Detection of pirfenidone and endogenous metabolites *in situ* in experimental fibrosis

To explore the distribution and effects of pirfenidone in fibrotic lung tissue, we induced experimental pulmonary fibrosis in mice using bleomycin. Pirfenidone (500 mg/kg) was administered once per day by oral gavage from day 7-14, based on the previously determined t_{max} in normal mouse tissues (18). On day 14, mice were sacrificed 45 min after final pirfenidone administration, and lung tissue was harvested. Histological analysis of bleomycin-treated samples revealed destruction of normal tissue architecture, excessive accumulation of extracellular matrix (ECM), and decreased lung compliance compared with PBS-treated controls (figure 1a and b). In bleomycin+pirfenidone-treated mice, we observed less pronounced lung fibrosis and significantly improved lung function, as demonstrated by improved compliance than observed in bleomycin-treated animals (figure 1a and b). The pirfenidone metabolites 5-hydroxymethyl pirfenidone (m/z 202.0863) and 5-carboxy pirfenidone (m/z 216.0655) were globally more abundant in lung tissue from bleomycin+pirfenidone-treated mice than unaffected controls treated with pirfenidone

(figure 1c). Notably, we observed increased pirfenidone accumulation in conserved areas of fibrotic lungs from bleomycin+pirfenidone-treated mice, corresponding to regions with lower COL1 content within fibrotic areas (figure 1f).

To identify alterations in endogenous metabolites, we performed *in situ* imaging of major members of key metabolic pathways in fibrotic lungs from bleomycin+pirfenidone-treated mice. We identified nucleotide derivatives, as well as central metabolic pathway and redox-related metabolites. For some (e.g. GMP, UMP, glucose 6-phosphate [G-6-P]), their distribution patterns correlated with fibrotic areas across micro-regions (figure 1d and e). We then performed unsupervised hierarchical clustering (27) (28) of metabolites in lungs from bleomycin+pirfenidone-treated animals and generated a segmentation map of fibrotic and non-fibrotic areas based on different MSI spectrum clusters (figure 1e). These data were in agreement with microscopic inspection conducted by histopathologists.

MALDI-FTICR-MSI analysis of glycolysis and TCA pathways after pirfenidone treatment

We next compared expression of several metabolites from glycolysis and the TCA, two central metabolic pathways, in lungs from animals in all treatment groups (figure 2). We observed that G-6-P is increased during fibrosis in bleomycin-treated mice, whereas 1,3-bisphosphoglycerate is decreased in lungs from bleomycin- and bleomycin+pirfenidone-treated animals; fructose 1,6-bisphosphate levels are unchanged. When pyruvate, which derives from 1,3-bisphosphoglycerate, enters the hexosamine biosynthesis pathway, it is transformed into UDP-N-acetyl glucosamine. UDP-N-acetyl glucosamine participates in hyaluronan synthesis (29), an ECM component that is highly produced by myofibroblasts in bleomycin-induced fibrosis and IPF (30). Here, we found significant enhancement of UDP-N-acetyl glucosamine in fibrotic lungs from bleomycin-treated mice. However, unlike UDP-N-acetyl glucosamine, citrate levels were similar in all groups. These data provide preliminary evidence for metabolic changes occurring in lungs during bleomycin-induced fibrosis and pirfenidone treatment in mice

Metabolic effects of pirfenidone treatment in bleomycin-induced lung fibrosis

We next performed metabolic pathway enrichment analysis, comparing PBS controls and bleomycin-induced fibrosis (figure 3a). Control regions were chosen from PBS-treated mice by selecting healthy, non-collapsed areas from each lung section. Fibrotic regions were selected from bleomycin-treated mice, based on histological features and the fibrotic clusters identified by spatial segmentation (figure 1e). In total, 1402 molecules were found to be significantly different between control and fibrotic tissue, with 409 molecules enriched and 993 molecules reduced in fibrotic regions. Furthermore, 536 of these were annotated in the METLIN Database; these were putatively assigned to 57 lipids (24 reduced and 33 enriched in fibrotic regions), 234 peptides (223 reduced and 11 enriched in fibrotic regions), and 245 other metabolites. Metabolites responsible for metabolic differentiation were then subjected to pathway enrichment analysis (figure 3, table 1). Regulated metabolites driving pathway significance are listed in supplementary table 1. We found glycolysis/gluconeogenesis metabolism was significantly reduced in pulmonary fibrosis, whereas ascorbate and aldarate metabolism, amino sugar and nucleotide sugar metabolism, the pentose phosphate pathway, pentose and glucuronate interconversions, and fructose and mannose metabolism were significantly enhanced in bleomycin-induced fibrosis (figure 3a, table 1, supplementary table 1).

To elucidate the pharmacometabolic effects of pirfenidone, a second comparison was performed on fibrotic animals treated with or without a 7-day oral dose of pirfenidone (figure 3b). From this analysis, 115 discriminative *m/z* species were identified. After database search and pathway analysis, ascorbate and aldarate metabolism, which were enhanced in bleomycin-induced fibrosis, were found to be down-regulated after pirfenidone treatment (figure 3b, table 1, supplementary table 1). This suggests a vital role for pirfenidone in switching systematic metabolite profiles in disease. Ascorbate contributes to efficient hydroxylation of hydroxyproline in elastin, collagen, and other ECM proteins with collagenous domains, thus supporting an important role of pirfenidone in modulating *de-novo* ECM production in bleomycin induced-fibrosis at the metabolic level.

To further clarify the role of pirfenidone during fibrosis, we performed metabolic pathway analysis on healthy mice treated with pirfenidone (PBS+pirfenidone). These data revealed high metabolic similarity between the PBS+pirfenidone group and mice treated with PBS

alone (figure 2, figure 3d, figure 4). This is consistent with our previous pharmacokinetic study of pirfenidone in healthy mouse tissues, in which we did not observe significant effects of pirfenidone, or its metabolites, on known metabolic pathways (18). We then compared lungs from fibrotic animals treated with bleomycin+pirfenidone and healthy mice treated with pirfenidone (PBS+pirfenidone). In total, 1076 molecules were significantly different between these groups, with 427 molecules enriched and 649 molecules reduced in fibrotic animals treated with pirfenidone. Pathway enrichment analysis identified multiple discriminative pathways, including glycolysis/gluconeogenesis, amino sugar and nucleotide sugar metabolism, the pentose phosphate pathway, pentose and glucuronate interconversions, and fructose and mannose metabolism (figure 3c). Notably, ascorbate and aldarate metabolism remained unchanged in fibrotic animals treated with pirfenidone compared with controls (PBS+pirfenidone). These results further support the effects of pirfenidone treatment on ascorbate and aldarate metabolism.

Next, we performed *in situ* detection of key metabolites from the major metabolic pathways reported above. We selected eight representative significantly regulated metabolites (four up, four down) that were strongly differentially regulated in fibrosis (figure 3d and e). Among the down-regulated metabolites in fibrosis, we included phosphoenol pyruvate, bisphosphoglycerate, phosphatidic acid, and phosphatidylethanolamine. Interestingly, phosphatidic acid and phosphatidylethanolamine were dramatically depleted in fibrosis, and these were partially restored in pirfenidone-treated. Conversely, ascorbic acid, G-6-P, N-acetylglucosamine phosphate, and UDP-N-acetyl-D-galactosamine are up-regulated during fibrosis. Remarkably, ascorbic acid is significantly decreased with pirfenidone treatment, supporting our pathway analysis.

Quantification of central pathway-related endogenous metabolites in healthy and fibrotic lung tissue

To further investigate metabolite dynamics in disease conditions, we compared the relative abundance of 25 endogenous metabolites (nucleotide derivatives, central pathway metabolites, prostaglandins, and redox-related metabolites) in control (PBS and PBS+pirfenidone treatment), bleomycin-treated, and bleomycin+pirfenidone-treated mice. Metabolite identification was performed using LC-MS on tissue MS/MS, or accurate mass

matching with databases (4 ppm mass accuracy, supplementary figures 2 and 3). Levels of 9/25 metabolites were significantly different between fibrotic and control tissue. Of the nucleotide derivatives, uridine monophosphate (UMP) and uridine diphosphate (UDP)-N-acetyl glucosamine were significantly increased in both fibrosis and pirfenidone-treated fibrosis when compared with controls (figure 4a). We also found that the prostaglandin (PG) pathway was highly regulated. While PG b₁ - PG a₁ was unchanged, PG E₂, PG G₂, PG G₁, and PG PGE₂ were significantly decreased in bleomycin- and bleomycin+pirfenidone-treated mice compared with controls (figure 4b). Lastly, we analysed metabolites from glycolysis and the TCA cycle and found that 1,3-biphosphoglycerate was significantly decreased in lungs from bleomycin- and bleomycin+pirfenidone-treated mice compared with controls, whereas G-6-P was increased in fibrotic and pirfenidone-treated fibrotic tissue (figure 4c).

Pharmacometabolic effects of pirfenidone in IPF

To determine whether this analysis is useful to identify metabolic footprints of fibrosis in human lungs, as well as the pharmacometabolic effect of pirfenidone in IPF, we performed pathway analysis of discriminative metabolites in human lungs from rejected donors, explanted lungs of treatment-naïve IPF patients, and IPF patients on pirfenidone treatment at time of transplantation. In a similar approach as described above, we initially compared donor with untreated IPF tissue, to identify metabolic pathways putatively modulated during fibrosis (figure 5, table 1, supplementary table 2). In total, 825 molecules were significantly different between donor and fibrotic tissue, with 480 molecules enriched and 345 molecules reduced in IPF. We then examined metabolic effects of pirfenidone in end-stage IPF by comparing explanted tissue from untreated and pirfenidone-treated IPF. From this analysis, 173 discriminative m/z species were identified (figure 5, supplementary table 2).

Metabolites responsible for metabolic differentiation were then subjected to pathway enrichment analysis; regulated metabolites driving pathway significance are listed in supplementary table 2. We identified pentose and glucuronate interconversions as pathways with the highest impact in IPF. Additionally, the ascorbate and aldarate pathways, as well as fructose and mannose metabolism, were upregulated in IPF, and vitamin B6 metabolism was increased in IPF compared with donor tissue (figure 5A, table 1,

supplementary table 2). Conversely, linoleic acid and inositol phosphate metabolism and the starch and sucrose pathways were down-regulated in IPF. Comparison of explanted tissue from untreated and pirfenidone-treated IPF (figure 5b, table 1, supplementary table 2) revealed signals from glycolysis/gluconeogenesis were enhanced with pirfenidone. We then performed *in situ* localization of key metabolites of the above-mentioned pathways (figure 5c and d) and confirmed both localization and significant reduction of D-myo-Inositol-triphosphate and phosphatidylcholine in IPF and pirfenidone-treated IPF. In contrast, we observed localization and a significant increase in 3-amino-2-oxopropylphosphate and cysteinyl-glycine IPF and pirfenidone-treated IPF.

Lastly, we measured relative abundance of 21 metabolites from several metabolic pathways (nucleotide derivatives, central pathway metabolites, prostaglandins, and redox-related metabolites) in control, IPF, and pirfenidone-treated IPF lungs; 5/21 were significantly regulated. Of the nucleotide derivatives, ATP was significantly decreased in IPF and pirfenidone-treated IPF compared with control tissue (figure 6a). From the redox pathway, both glutathione (GSH) and glutathione disulfide (GSSG) were significantly increased in pirfenidone-treated IPF compared with control tissue (figure 6a). The prostaglandin pathway was within the lower range of expression in humans, although PG G₂ was significantly increased in IPF compared to controls. From glycolysis and the TCA cycle, G-6-P was significantly increased in pirfenidone-treated IPF when compared with control tissue. Further, fructose 1,6-bisphosphate, which is involved in glycolysis/gluconeogenesis, was significantly down-regulated in IPF, suggesting deregulation of glycolysis/gluconeogenesis in this disease (figure 6c). Enhancement of the glycolysis/gluconeogenesis pathway upon pirfenidone administration (figure 5b) demonstrates a possible role for pirfenidone in restoring glycolysis in IPF.

Discussion

This proof-of-concept study demonstrated, for the first time, *in situ* metabolic alterations during fibrosis and the pharmacometabolic effect of pirfenidone on fibrotic tissue of mice and humans. Specifically, we found increased levels of pirfenidone and related metabolites in fibrotic tissue using high-resolution *in situ* mass spectrometry. We detected mass spectra of fibrotic areas, to assess metabolite composition in specific regions of interest. Using this

technology, we were then able to dissect metabolic pathways simultaneously in multiple samples and determine spatial distribution, as well as quantify intensity of detection. Lastly, we identified overlapping and exclusive metabolic fingerprints that putatively characterize fibrotic responses in humans and mice, together with pharmacometabolic responses to pirfenidone in fibrosis.

Due to the relatively small number of mice in each treatment group (n=3), this should be viewed as a proof-of-concept study, exploring the utility of MALDI-FTICR-MSI for detection of metabolites in a mouse model of pulmonary fibrosis. To demonstrate statistical significance and reproducibility of our experiments, we performed hierarchical clustering and partial least squares-discriminant analysis (PLS-DA) (supplementary figure 1). These data demonstrate clear separations between PBS, bleomycin, and bleomycin+pirfenidone-treated groups, and underscore the power of this approach.

Metabolomics is the study of global endogenous metabolite profiles generated by specific cellular processes. The presented metabolomic analyses has the potential to enhance understanding of fibrotic processes, promote discovery of diagnostic biomarkers, identify novel targets, and improve current therapies. Critically, our data demonstrate that MALDI-FTICR-MSI can provide the microscopic and molecular analytic capabilities necessary for understanding the spatio-molecular features of complex microenvironments in IPF tissue.

Investigation of the distribution of pirfenidone and its related drug metabolites in the lung revealed 5-hydroxymethyl pirfenidone (m/z 202.0863) and 5-carboxy pirfenidone (m/z 216.0655) are globally more abundant in fibrotic lungs. However in fibrotic lungs, they were abundantly localized in less affected areas, with lower COL1 expression. This suggests the distribution, and possibly the metabolism, of pirfenidone are enhanced in fibrosis, and accumulation in affected areas might be required for its anti-fibrotic effects. In lung fibroblasts, 5-hydroxymethyl pirfenidone and 5-carboxy pirfenidone inhibit TGF- β -induced collagen synthesis, demonstrating these metabolites have anti-fibrotic activities (31).

Using ultra-sensitive MSI, we detected, and simultaneously visualized, thousands of endogenous metabolites in mouse and human lung sections, from diseased and control tissues. These include nucleotide derivatives, as well as central metabolic pathway metabolites, redox-related metabolites, and prostaglandins, among others. We observed

that intermediates in glycolysis, nucleotide metabolism, and the pentose phosphate pathway are altered in fibrotic regions compared with healthy lungs. It was previously shown that glycolysis is altered in IPF (16). Kottmann *et al.* further suggested that dysregulated glycolysis results in elevated lactate levels, which may facilitate disease progression (32). This metabolic switch towards oxidative pentose phosphate pathway in fibrosis might indicate the elevated energy demand and higher energy consumption present in fibrosis. Consistent with this, we found lower levels of ATP in IPF patients. Similarly, extracellular ATP is decreased in bronchoalveolar lavage fluid from IPF samples (33), and others have shown decreased intracellular ATP in IPF tissue (17), which may result from accumulation of dysfunctional mitochondria that promote fibrosis (34). Collectively, these findings suggest an alternative energy cascade related to altered glycolysis in IPF.

Other metabolites identified in our dataset are related to redox mechanisms. Interestingly, we found unchanged levels of GSH and GSSG in bleomycin-induced pulmonary fibrosis, whereas these are increased in pirfenidone-treated IPF patients. In mice, levels of GSH and GSSG are suppressed by overexpression of TGF- β (35). We speculate that recovery of GSH and GSSG levels in IPF might indicate a role for pirfenidone in modulating the redox imbalance that contributes to persistent fibrosis (36).

Remarkably, we observed increased ascorbate and aldarate metabolism in both mice and humans with fibrosis. This is consistent with the enhancement in collagen metabolism and production observed in organ fibrosis. In mice, ascorbate and aldarate metabolism decrease after pirfenidone treatment. Ascorbate is a crucial co-substrate for enzymes catalysing post-translational hydroxylation of prolyl and lysyl residues necessary for thermostability of the collagen triple helix and extracellular cross-linking of collagen fibres (37, 38), making it critical for collagen synthesis and processing. Thus, enhancement of ascorbate and aldarate metabolism during fibrosis, and the corresponding decrease after pirfenidone administration, are indicative of its anti-fibrotic activity. These data are also consistent with the effect of pirfenidone on collagen processing, and support its role in inhibiting collagen fibril formation in IPF fibroblasts (39).

Significant alteration of lipids in fibrotic regions is consistent with recent studies demonstrating that lipids, particularly phospholipids, are increased in fibrosis and can act as

mediators in lipid-signaling pathways (40-43). Additionally, prostaglandins, which are suggested to have anti-fibrotic activities in lung injury (44), were also reduced in fibrotic regions, implying these may serve as indicators, and potentially relevant targets, for pulmonary fibrosis treatment.

Pathway enrichment analysis further revealed putative overlapping, as well as, distinctive features in mouse and human fibrosis (figure 3, table 1, supplementary tables 1 and 2), and several factors may account for these differences. First, we note bleomycin-induced pulmonary fibrosis is a self-resolving, easily manipulated model, which does not fully recapitulate human IPF, although it does show strong commonalities on distinct levels, supporting continuous use for preclinical testing (45). Second, pirfenidone treatment in mice occurred from disease initiation to peak of fibrosis, whereas our IPF cohort was at end-stage disease, requiring transplantation. Thus, our data may also reflect important differences in treatment responses at different disease stages.

IPF is a multifactorial and complex disease, and bleomycin-induced fibrosis remains the most studied model of lung fibrosis. Kinetic analyses to study the metabolic effects of pirfenidone treatment, and metabolic pathway modifications occurring early after pirfenidone administration, are therefore limited to this model. For example, pirfenidone and its metabolites are maximally detectable in lungs 45 min post-administration (18). Thus, we successfully detected increased levels of pirfenidone and its related metabolites in mouse, but not human, fibrotic lungs. This may result from timely, controlled drug administration in mice, which is difficult to recapitulate clinically, in pre-transplanted patients immediately preceding surgical procedures. Despite the factors mentioned above, with the introduction of transbronchial cryobiopsies for earlier diagnosis of diffuse parenchymal lung diseases (46), differences can be minimized, and the applicability of MALDI imaging for metabolite profiling or pharmacometabolic drug responses should be considered.

Collectively, our findings suggest metabolic profiles are altered in regions affected by pulmonary fibrosis. Although results are preliminary, based on this proof-of-concept study, we propose that the combination of pharmaco- and metabolomics utilized in this study, may ultimately lead to improved understanding of both disease mechanisms of IPF and the

mechanism of action of pirfenidone. Moreover, elucidating pirfenidone-associated metabolism and its cellular mechanism of action may facilitate prediction of individual responses to anti-fibrotic drugs. Label-free MALDI-MSI techniques allow simultaneous detection, visualization, and quantification of both exogenous (drugs and related metabolites) and endogenous metabolites, providing competitive advantages over traditional analytical techniques. Thus, we anticipate MALDI-MSI techniques for determining spatiotemporal behaviours of drugs and endogenous metabolites will be broadly applicable to drug efficacy studies and elucidating the metabolism of bioactive small molecules involved in fibrosis and other pathological conditions.

References

1. Fernandez IE, Eickelberg O. New cellular and molecular mechanisms of lung injury and fibrosis in idiopathic pulmonary fibrosis. *Lancet* 2012; 380: 680-688.
2. Schaefer CJ, Ruhrmund DW, Pan L, Seiwert SD, Kossen K. Antifibrotic activities of pirfenidone in animal models. *European respiratory review : an official journal of the European Respiratory Society* 2011; 20: 85-97.
3. Lasky J. Pirfenidone. *IDrugs* 2004; 7: 166-172.
4. Raghu G, Collard HR, Egan JJ, Martinez FJ, Behr J, Brown KK, Colby TV, Cordier JF, Flaherty KR, Lasky JA, Lynch DA, Ryu JH, Swigris JJ, Wells AU, Ancochea J, Bouros D, Carvalho C, Costabel U, Ebina M, Hansell DM, Johkoh T, Kim DS, King TE, Jr., Kondoh Y, Myers J, Muller NL, Nicholson AG, Richeldi L, Selman M, Dudden RF, Griss BS, Protzko SL, Schunemann HJ, Fibrosis AEJACoIP. An official ATS/ERS/JRS/ALAT statement: idiopathic pulmonary fibrosis: evidence-based guidelines for diagnosis and management. *Am J Respir Crit Care Med* 2011; 183: 788-824.
5. Carter NJ. Pirfenidone: in idiopathic pulmonary fibrosis. *Drugs* 2011; 71: 1721-1732.
6. Kakugawa T, Mukae H, Hayashi T, Ishii H, Abe K, Fujii T, Oku H, Miyazaki M, Kadota J, Kohno S. Pirfenidone attenuates expression of HSP47 in murine bleomycin-induced pulmonary fibrosis. *The European respiratory journal* 2004; 24: 57-65.
7. Cornett DS, Frappier SL, Caprioli RM. MALDI-FTICR imaging mass spectrometry of drugs and metabolites in tissue. *Analytical chemistry* 2008; 80: 5648-5653.
8. Römpf A, Guenther S, Takats Z, Spengler B. Mass spectrometry imaging with high resolution in mass and space (HR(2) MSI) for reliable investigation of drug compound distributions on the cellular level. *Analytical and bioanalytical chemistry* 2011; 401: 65-73.
9. Castellino S, Groseclose MR, Wagner D. MALDI imaging mass spectrometry: bridging biology and chemistry in drug development. *Bioanalysis* 2011; 3: 2427-2441.
10. Kim YH, Fujimura Y, Hagihara T, Sasaki M, Yukihiro D, Nagao T, Miura D, Yamaguchi S, Saito K, Tanaka H, Wariishi H, Yamada K, Tachibana H. In situ label-free imaging for visualizing the biotransformation of a bioactive polyphenol. *Scientific reports* 2013; 3: 2805.
11. Miura D, Fujimura Y, Wariishi H. In situ metabolomic mass spectrometry imaging: recent advances and difficulties. *Journal of proteomics* 2012; 75: 5052-5060.
12. Balluff B, Schone C, Hofler H, Walch A. MALDI imaging mass spectrometry for direct tissue analysis: technological advancements and recent applications. *Histochemistry and cell biology* 2011; 136: 227-244.
13. Abrosimov LI, Karasik VE, Beliakova IP. [Hygienic principles of physical load standardizing in physical education of school children]. *Vestnik Rossiiskoi akademii meditsinskikh nauk / Rossiiskaia akademiia meditsinskikh nauk* 1993: 13-19.
14. Walch A, Rauser S, Deininger SO, Hofler H. MALDI imaging mass spectrometry for direct tissue analysis: a new frontier for molecular histology. *Histochemistry and cell biology* 2008; 130: 421-434.
15. Aichler M, Borgmann D, Krumsiek J, Buck A, MacDonald PE, Fox JEM, Lyon J, Light PE, Keipert S, Jastroch M, Feuchtinger A, Mueller NS, Sun N, Palmer A, Alexandrov T, Hrabe de Angelis M, Neschen S, Tschop MH, Walch A. N-acyl Taurines and Acylcarnitines Cause an Imbalance in Insulin Synthesis and Secretion Provoking beta Cell Dysfunction in Type 2 Diabetes. *Cell metabolism* 2017; 25: 1334-1347 e1334.
16. Zhao YD, Yin L, Archer S, Lu C, Zhao G, Yao Y, Wu L, Hsin M, Waddell TK, Keshavjee S, Granton J, de Perrot M. Metabolic heterogeneity of idiopathic pulmonary fibrosis: a metabolomic study. *BMJ Open Respiratory Research* 2017; 4.
17. Kang YP, Lee SB, Lee JM, Kim HM, Hong JY, Lee WJ, Choi CW, Shin HK, Kim DJ, Koh ES, Park CS, Kwon SW, Park SW. Metabolic Profiling Regarding Pathogenesis of Idiopathic Pulmonary Fibrosis. *Journal of proteome research* 2016; 15: 1717-1724.

18. Sun N, Fernandez IE, Wei M, Wu Y, Aichler M, Eickelberg O, A. W. Pharmacokinetic and pharmacometabolomic study of pirfenidone in normal mice tissues using high mass resolution MALDI-FTICR-mass spectrometry imaging. *Histochemistry and cell biology* 2015.
19. Fernandez IE, Amarie OV, Mutze K, Konigshoff M, Yildirim AO, Eickelberg O. Systematic phenotyping and correlation of biomarkers with lung function and histology in lung fibrosis. *American journal of physiology Lung cellular and molecular physiology* 2016; 310: L919-927.
20. Verleden SE, Vasilescu DM, Willems S, Ruttens D, Vos R, Vandermeulen E, Hostens J, McDonough JE, Verbeken EK, Verschakelen J, Van Raemdonck DE, Rondelet B, Knoop C, Decramer M, Cooper J, Hogg JC, Verleden GM, Vanaudenaerde BM. The site and nature of airway obstruction after lung transplantation. *American journal of respiratory and critical care medicine* 2014; 189: 292-300.
21. Boon M, Verleden SE, Bosch B, Lammertyn EJ, McDonough JE, Mai C, Verschakelen J, Kemner-van de Corput M, Tiddens HA, Proesmans M, Vermeulen FL, Verbeken EK, Cooper J, Van Raemdonck DE, Decramer M, Verleden GM, Hogg JC, Dupont LJ, Vanaudenaerde BM, De Boeck K. Morphometric Analysis of Explant Lungs in Cystic Fibrosis. *American journal of respiratory and critical care medicine* 2016; 193: 516-526.
22. Sun N, Ly A, Meding S, Witting M, Hauck SM, Ueffing M, Schmitt-Kopplin P, Aichler M, Walch A. High-resolution metabolite imaging of light and dark treated retina using MALDI-FTICR mass spectrometry. *Proteomics* 2014; 14: 913-923.
23. Buck A, Ly A, Balluff B, Sun N, Gorzolka K, Feuchtinger A, Janssen KP, Kuppen PJ, van de Velde CJ, Weirich G, Erlmeier F, Langer R, Aubele M, Zitzelsberger H, Aichler M, Walch A. High-resolution MALDI-FT-ICR MS Imaging for the analysis of metabolites from formalin-fixed paraffin-embedded clinical tissue samples. *The Journal of pathology* 2015.
24. Palmer A, Phapale P, Chernyavsky I, Lavigne R, Fay D, Tarasov A, Kovalev V, Fuchser J, Nikolenko S, Pineau C, Becker M, Alexandrov T. FDR-controlled metabolite annotation for high-resolution imaging mass spectrometry. *Nature methods* 2017; 14: 57-60.
25. Wishart DS, Tzur D, Knox C, Eisner R, Guo AC, Young N, Cheng D, Jewell K, Arndt D, Sawhney S, Fung C, Nikolai L, Lewis M, Coutouly MA, Forsythe I, Tang P, Shrivastava S, Jeroncic K, Stothard P, Amegbey G, Block D, Hau DD, Wagner J, Miniaci J, Clements M, Gebremedhin M, Guo N, Zhang Y, Duggan GE, Macinnis GD, Weljie AM, Dowlatabadi R, Bamforth F, Clive D, Greiner R, Li L, Marrie T, Sykes BD, Vogel HJ, Querengesser L. HMDB: the Human Metabolome Database. *Nucleic acids research* 2007; 35: D521-526.
26. Xia J, Wishart DS. MetPA: a web-based metabolomics tool for pathway analysis and visualization. *Bioinformatics* 2010; 26: 2342-2344.
27. Alexandrov T, Becker M, Deininger SO, Ernst G, Wehder L, Grasmair M, von Eggeling F, Thiele H, Maass P. Spatial segmentation of imaging mass spectrometry data with edge-preserving image denoising and clustering. *Journal of proteome research* 2010; 9: 6535-6546.
28. Alexandrov T, Becker M, Guntinas-Lichius O, Ernst G, von Eggeling F. MALDI-imaging segmentation is a powerful tool for spatial functional proteomic analysis of human larynx carcinoma. *Journal of cancer research and clinical oncology* 2013; 139: 85-95.
29. Albeiroti S, Soroosh A, de la Motte CA. Hyaluronan's Role in Fibrosis: A Pathogenic Factor or a Passive Player? *BioMed research international* 2015; 2015: 790203.
30. Li Y, Jiang D, Liang J, Meltzer EB, Gray A, Miura R, Wogensen L, Yamaguchi Y, Noble PW. Severe lung fibrosis requires an invasive fibroblast phenotype regulated by hyaluronan and CD44. *The Journal of experimental medicine* 2011; 208: 1459-1471.
31. Togami K, Kanehira Y, Tada H. Possible involvement of pirfenidone metabolites in the antifibrotic action of a therapy for idiopathic pulmonary fibrosis. *Biological & pharmaceutical bulletin* 2013; 36: 1525-1527.
32. Kottmann RM, Kulkarni AA, Smolnycki KA, Lyda E, Dahanayake T, Salibi R, Honnons S, Jones C, Isern NG, Hu JZ, Nathan SD, Grant G, Phipps RP, Sime PJ. Lactic acid is elevated in idiopathic pulmonary fibrosis and induces myofibroblast differentiation via pH-dependent activation of

- transforming growth factor-beta. *American journal of respiratory and critical care medicine* 2012; 186: 740-751.
33. Riteau N, Gasse P, Fauconnier L, Gombault A, Couegnat M, Fick L, Kanellopoulos J, Quesniaux VF, Marchand-Adam S, Crestani B, Ryffel B, Couillin I. Extracellular ATP is a danger signal activating P2X7 receptor in lung inflammation and fibrosis. *American journal of respiratory and critical care medicine* 2010; 182: 774-783.
 34. Bueno M, Lai YC, Romero Y, Brands J, St Croix CM, Kamga C, Corey C, Herazo-Maya JD, Sembrat J, Lee JS, Duncan SR, Rojas M, Shiva S, Chu CT, Mora AL. PINK1 deficiency impairs mitochondrial homeostasis and promotes lung fibrosis. *The Journal of clinical investigation* 2015; 125: 521-538.
 35. Lu HI, Huang TH, Sung PH, Chen YL, Chua S, Chai HY, Chung SY, Liu CF, Sun CK, Chang HW, Zhen YY, Lee FY, Yip HK. Administration of antioxidant peptide SS-31 attenuates transverse aortic constriction-induced pulmonary arterial hypertension in mice. *Acta pharmacologica Sinica* 2016; 37: 589-603.
 36. Kurundkar A, Thannickal VJ. Redox mechanisms in age-related lung fibrosis. *Redox biology* 2016; 9: 67-76.
 37. Hata R, Senoo H. L-ascorbic acid 2-phosphate stimulates collagen accumulation, cell proliferation, and formation of a three-dimensional tissuelike substance by skin fibroblasts. *Journal of cellular physiology* 1989; 138: 8-16.
 38. Murad S, Tajima S, Johnson GR, Sivarajah S, Pinnell SR. Collagen synthesis in cultured human skin fibroblasts: effect of ascorbic acid and its analogs. *The Journal of investigative dermatology* 1983; 81: 158-162.
 39. Knuppel L, Ishikawa Y, Aichler M, Heinzelmann K, Hatz R, Behr J, Walch A, Bachinger HP, Eickelberg O, Staab-Weijnitz CA. A Novel Antifibrotic Mechanism of Nintedanib and Pirfenidone. Inhibition of Collagen Fibril Assembly. *American journal of respiratory cell and molecular biology* 2017; 57: 77-90.
 40. Castellino FV. Lipids and eicosanoids in fibrosis: emerging targets for therapy. *Current opinion in rheumatology* 2012; 24: 649-655.
 41. Mouratis MA, Aidinis V. Modeling pulmonary fibrosis with bleomycin. *Current opinion in pulmonary medicine* 2011; 17: 355-361.
 42. Tager AM, LaCamera P, Shea BS, Campanella GS, Selman M, Zhao Z, Polosukhin V, Wain J, Karimi-Shah BA, Kim ND, Hart WK, Pardo A, Blackwell TS, Xu Y, Chun J, Luster AD. The lysophosphatidic acid receptor LPA1 links pulmonary fibrosis to lung injury by mediating fibroblast recruitment and vascular leak. *Nature medicine* 2008; 14: 45-54.
 43. Patel RB, Kotha SR, Sherwani SI, Sliman SM, Gurney TO, Loar B, Butler SO, Morris AJ, Marsh CB, Parinandi NL. Pulmonary fibrosis inducer, bleomycin, causes redox-sensitive activation of phospholipase D and cytotoxicity through formation of bioactive lipid signal mediator, phosphatidic acid, in lung microvascular endothelial cells. *International journal of toxicology* 2011; 30: 69-90.
 44. Huang SK, Peters-Golden M. Eicosanoid lipid mediators in fibrotic lung diseases: ready for prime time? *Chest* 2008; 133: 1442-1450.
 45. Jenkins RG, Moore BB, Chambers RC, Eickelberg O, Konigshoff M, Kolb M, Laurent GJ, Nanthakumar CB, Olman MA, Pardo A, Selman M, Sheppard D, Sime PJ, Tager AM, Tatler AL, Thannickal VJ, White ES, Cell ATSAoR, Molecular B. An Official American Thoracic Society Workshop Report: Use of Animal Models for the Preclinical Assessment of Potential Therapies for Pulmonary Fibrosis. *American journal of respiratory cell and molecular biology* 2017; 56: 667-679.
 46. Hetzel J, Maldonado F, Ravaglia C, Wells AU, Colby TV, Tomassetti S, Ryu JH, Fruchter O, Piciucchi S, Dubini A, Cavazza A, Chilosi M, Sverzellati N, Valeyre D, Leduc D, Walsh SLF, Gasparini S, Hetzel M, Hagemeyer L, Haentschel M, Eberhardt R, Darwiche K, Yarmus LB, Torrego A, Krishna G, Shah PL, Annema JT, Herth FJF, Poletti V. Transbronchial Cryobiopsies for the

Diagnosis of Diffuse Parenchymal Lung Diseases: Expert Statement from the Cryobiopsy Working Group on Safety and Utility and a Call for Standardization of the Procedure. *Respiration*; international review of thoracic diseases 2018; 95: 188-200.

Acknowledgments

The study was funded by Helmholtz Zentrum München (TKP-Project), the German Centre for Lung Research (DZL), the Ministry of Education and Research of the Federal Republic of Germany (BMBF; 01ZX1310B and 01KT1615), and the Deutsche Forschungsgemeinschaft (Grant Nos.: HO 1254/3-1, SFB 824 C4, CRC/Transregio 205/1 "The Adrenal: Central Relay in Health and Disease") to A.W. The authors would like to thank Claudia-Marieke Pflüger, Ulrike Buchholz, Gabriele Mettenleiter, and Andreas Voss from the Research Unit Analytical Pathology, as well as Constanze Heise and Daniela Dietel from the Comprehensive Pneumology Centre, for providing technical assistance.

Author Contributions

A.W., O.E., N.S., and I.E.F. designed the study. N.S., I.E.F., Mian W., and Michael W. performed the experiments. S.E.V. provided lung tissues from healthy donors, IPF, and pirfenidone-treated IPF lung tissue. N.S. and I.E.F. drafted the manuscript. I.E.F., N.S., A.W., O.E., and M.A. analysed and interpreted the results. I.E.F., N.S., A.W., O.E., S.E.V., M.A., Mian W., Michael W., and P.S.K. drafted and edited the manuscript for important intellectual content. G.B., and A.F. supported immunofluorescence experiments.

Competing financial interests

The authors have declared no conflicts of interest.

Figure captions

Figure 1. Pirfenidone detection in bleomycin-induced pulmonary fibrosis mice lungs. a) Haematoxylin and Eosin (H&E) staining of sectioned lungs from mice treated with phosphate-buffered saline (PBS), PBS+pirfenidone (PBS+PFD), bleomycin to induce fibrosis, and bleomycin+pirfenidone (B+PFD). b) Lung compliance measurements of mice from each treatment group. Data are shown as mean \pm standard deviation (SD), and asterisks (*, **, ***) indicate significant differences ($p \leq 0.05$, 0.01 , 0.001 , respectively). c) Left panel: mass spectrometry imaging (MSI) distribution of pirfenidone and its related metabolites, 5-hydroxymethyl pirfenidone and 5-carboxy pirfenidone, in lungs from PBS+PFD and B+PFD-treated mice. Right panel: relative quantification of pirfenidone and related metabolites in lungs from PBS+PFD and B+PFD-treated mice. d) Heterogeneous distribution pattern of central pathway-related endogenous metabolites in lung tissue from B+PFD-treated mice: UDP-GlcNAc (UDP-N-acetylglucosamine), G-6-P (glucose-6-phosphate), F-1,6-P (fructose-1,6-bisphosphate), glycerol-P (glycerol monophosphate), GSSG (glutathione disulphide). e) H&E images with zoomed regions of non-fibrotic and fibrotic tissue are illustrated. Spatial segmentation of histological components through unsupervised hierarchical clustering reflects the histological components of fibrotic (blue) and non-fibrotic area (pink). f) Immunofluorescence staining for collagen type 1 in sectioned lungs from the B+PFD-treated group.

Figure 2. Analysis of glycolysis and TCA cycle metabolism by MALDI-FTICR-MSI in fibrotic mice. H&E sections of lungs treated with PBS, PBS+pirfenidone (PBS+PFD), bleomycin, and bleomycin+pirfenidone (B+PFD) are shown in the top left. Representative metabolite images of selected steps of the glycolysis and TCA cycle are shown on the right, and representative images of selected metabolites are shown in green font.

Figure 3. Pathway analysis of discriminative metabolic alterations in experimental fibrosis with and without pirfenidone treatment. Metabolic pathways are represented as circles according to their scores from enrichment (vertical axis) and topology analyses (pathway impact, horizontal axis) using MetaboAnalyst. a) Discriminative pathways in bleomycin-induced fibrosis compared with PBS controls. b) Discriminative pathways in bleomycin-induced fibrosis upon pirfenidone treatment. c) Discriminative pathways in

bleomycin-induced fibrosis upon pirfenidone treatment compared with the PBS+pirfenidone-treated group. d) H&E sections of lungs treated with PBS, PBS+pirfenidone (PBS+PFD), bleomycin, and bleomycin+pirfenidone (B+PFD) are shown in the middle. On the right, from top to bottom, representative images of metabolites reduced in fibrosis: phosphoenol pyruvate (m/z 166.9750), bisphosphoglycerate (m/z 264.9525), phosphatidic acid (m/z 647.4675), phosphatidylethanolamine (m/z 746.5140). On the left, from top to bottom, representative images of metabolites enhanced in fibrosis: ascorbic acid (m/z 175.0250), glucose-6-phosphate (m/z 259.0230), N-acetylglucosamine-phosphate (m/z 300.0495), UDP-N-acetyl-D-galactosamine (606.0755). e) Relative quantification of metabolites depicted in panel d) in mice treated with PBS, PBS+PFD, bleomycin, and B+PFD. One-way analysis of variance (ANOVA) was used for statistical analysis, with the Bonferroni *post-hoc* test. Asterisks (*, **, ***) indicate significant differences ($p \leq 0.05$, 0.01, 0.001, respectively) between PBS and treated group.

Figure 4. Relative abundance of endogenous tissue metabolites in mice treated with PBS, PBS+pirfenidone (PBS+PFD), bleomycin, or bleomycin+pirfenidone (B+PFD). Metabolites are grouped as a) nucleotide derivatives and redox-associated metabolites, b) prostaglandins, and c) glycolysis and the TCA cycle. Data are shown as the mean \pm SD (n=3) and represent the relative concentration of each group. One-way ANOVA was used for statistical analysis, with the Bonferroni *post-hoc* test. Asterisks (*, **, ***) indicate significant differences ($p \leq 0.05$, 0.01, 0.001, respectively) between PBS and treated groups. G-6-P (glucose-6-phosphate); F-1,6-P (fructose-1,6-bisphosphate); glycerol-P (glycerol monophosphate); GSSG (glutathione disulphide).

Figure 5. Pathway analysis of discriminative metabolic alterations in IPF patients with and without pirfenidone treatment. Metabolic pathways are represented as circles according to their scores from enrichment (vertical axis) and topology analyses (pathway impact, horizontal axis) using MetaboAnalyst. a) Discriminative pathways in IPF compared with donor. b) Discriminative pathways in IPF after pirfenidone therapy. c) H&E sections of explanted lungs from donors, untreated IPF, or pirfenidone-treated IPF (IPF+PFD) patients are shown in the top. On the right, from top to bottom, representative images of metabolites reduced in IPF: D-myo-Inositoltriphosphate (m/z 418.9565), phosphatidylcholine (m/z 718.5410). On the left, from top to bottom, representative images

of metabolites enhanced in IPF: 3-Amino-2-oxopropylphosphate (m/z 168.0070), cyteinyglycine (m/z 177.0340). D) Relative quantification of the depicted metabolites in donor, IPF, and pirfenidone-treated IPF (IPF+PFD). One-way ANOVA was used for statistical analysis, with the Bonferroni *post-hoc* test. Asterisks (*, **, ***) indicate significant differences ($p \leq 0.05$, 0.01, 0.001, respectively) between donor and treated group.

Figure 6. Relative abundance of endogenous tissue metabolites from donor, IPF, and pirfenidone-treated IPF patients. Metabolites are grouped as a) nucleotide derivatives and redox-associated metabolites, b) prostaglandins, and c) glycolysis and the TCA cycle. Data are shown as the mean \pm SD (n=3) and represent the relative concentration of each group. One-way ANOVA was used for statistical analysis, with the Bonferroni *post-hoc* test. Asterisks (*) indicate significant differences ($p \leq 0.05$) between control and disease. G-6-P (glucose-6-phosphate); F-1,6-P (fructose-1,6-bisphosphate); glycerol-P (glycerol monophosphate); GSSG (glutathione disulphide).

Table 1. Modulated metabolite pathways in mice and human during fibrosis and upon pirfenidone treatment.

Table 1

	Discriminative pathways	Bleomycine induced-pulmonary fibrosis	IPF
Reduced in fibrosis	Glycolysis or Gluconeogenesis	yes	no
	Linoleic acid metabolism	no	yes
	Inositol phosphate metabolism	no	yes
	Starch and sucrose metabolism	no	yes
Enhanced in fibrosis	Pentose and glucuronate interconversions	yes	yes
	Ascorbate and aldarate metabolism	yes	yes
	Amino sugar and nucleotide sugar metabolism	yes	no
	Pentose phosphate pathway	yes	no
	Fructose and mannose metabolism	yes	yes
	Vitamin B6 metabolism	no	yes
	Glutathione metabolism	no	yes
Reduced upon Pirfenidone	Ascorbate and aldarate metabolism	yes	no
Enhanced upon Pirfenidone	Glycolysis or Gluconeogenesis	no	yes

Figure 1

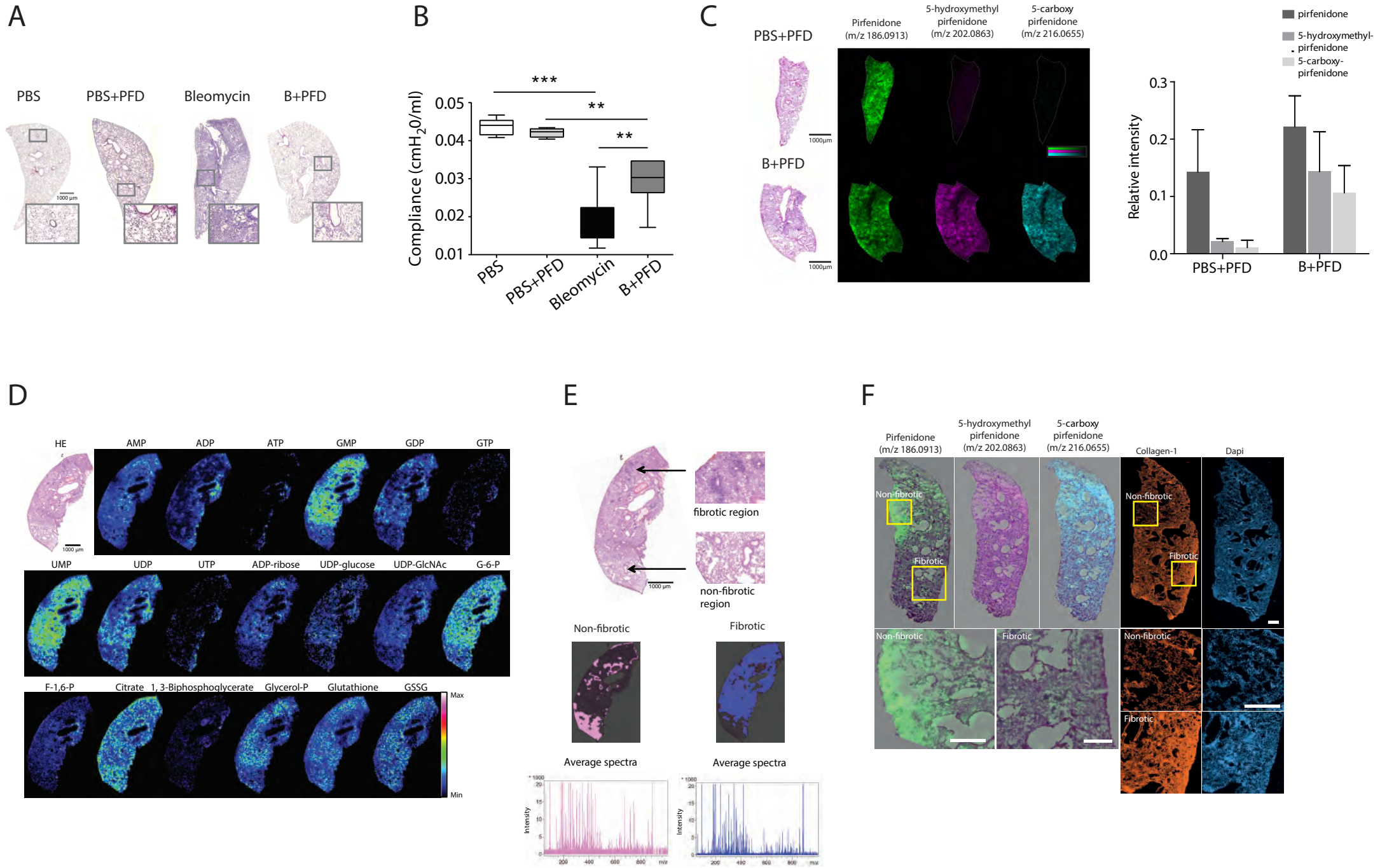


Figure 2

Glycolysis

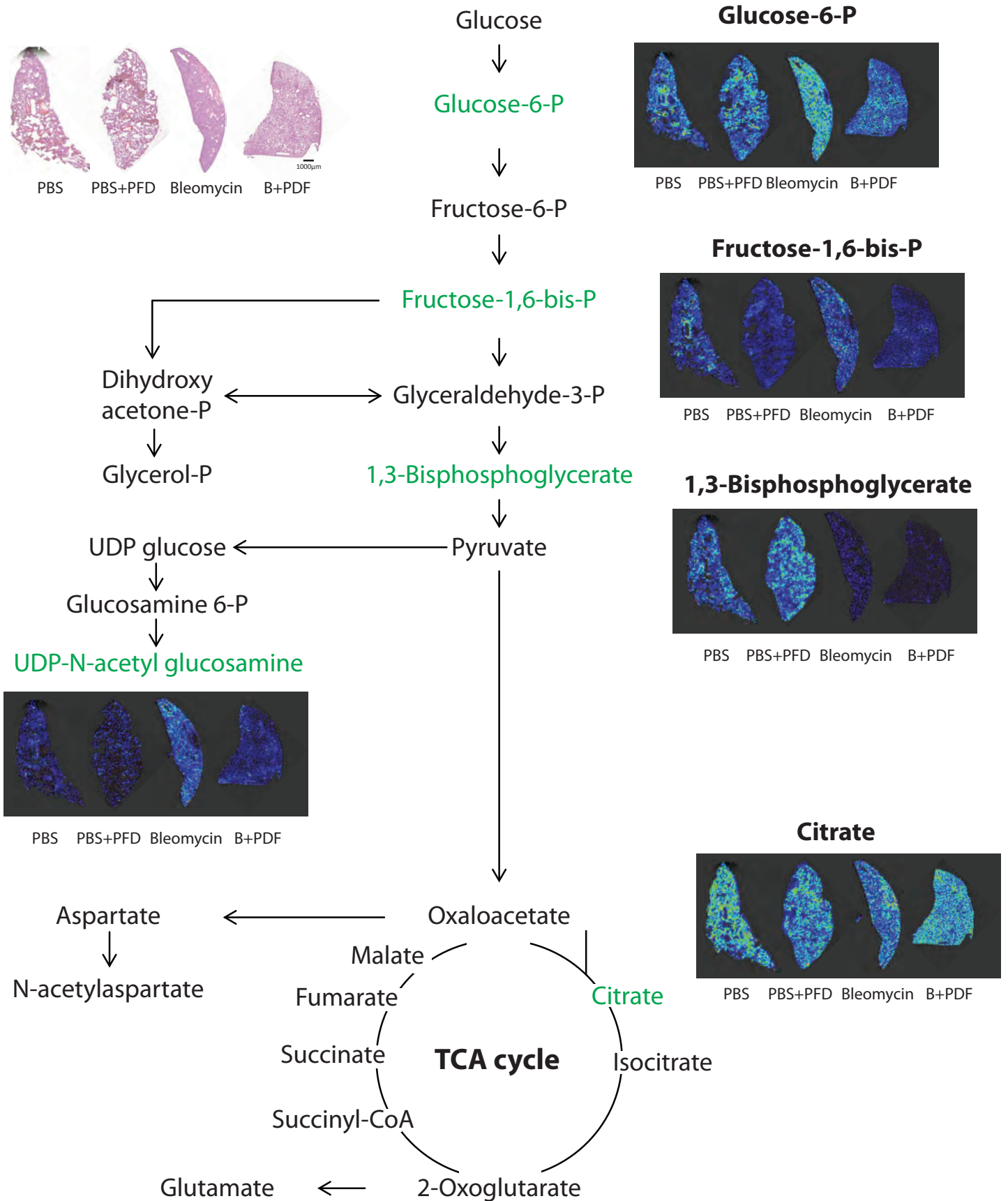
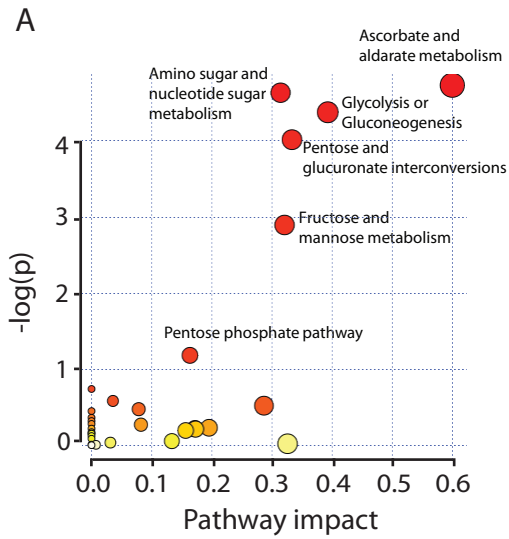
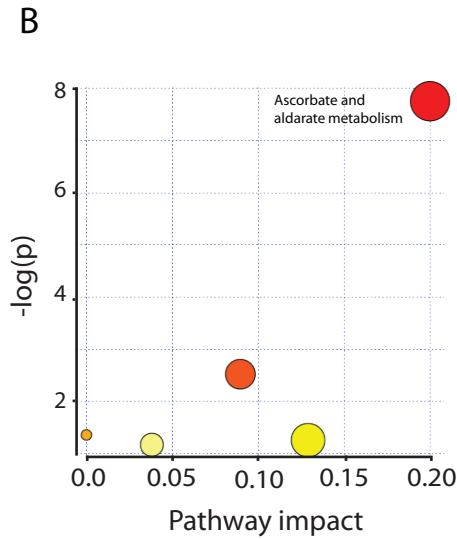


Figure 3

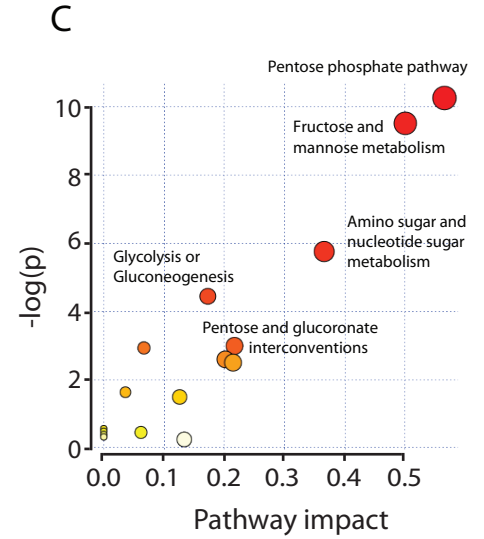
PBS vs. Bleomycin



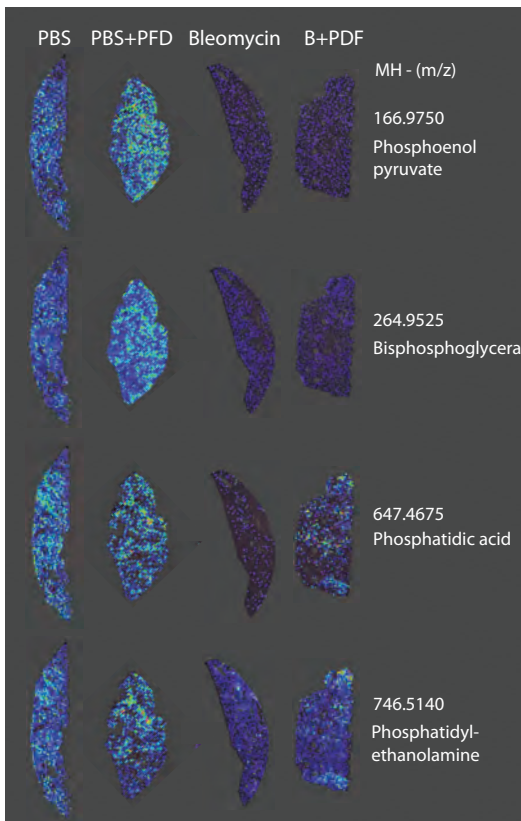
Bleomycin vs. Bleomycin+PFD



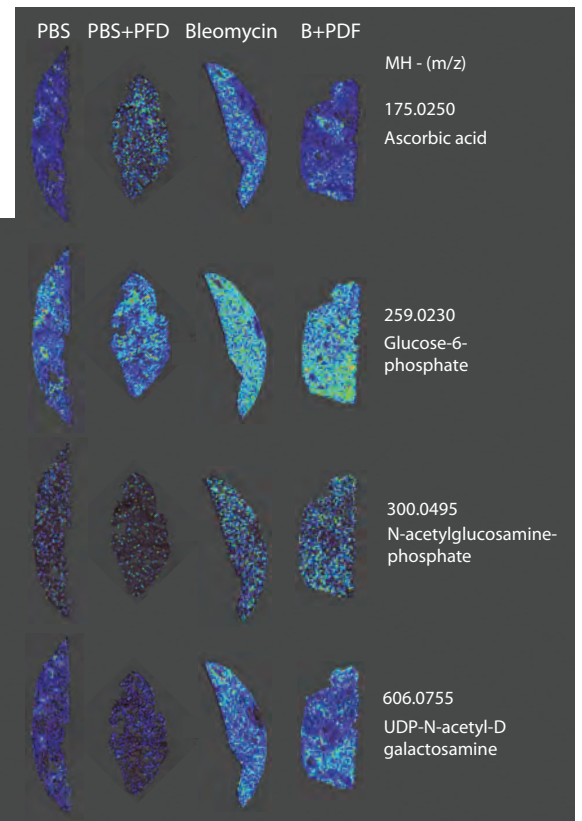
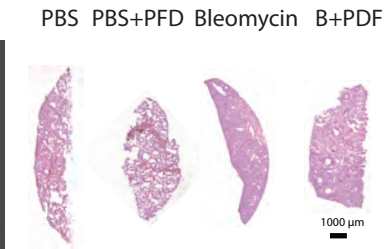
PBS+PFD vs. Bleomycin+PFD



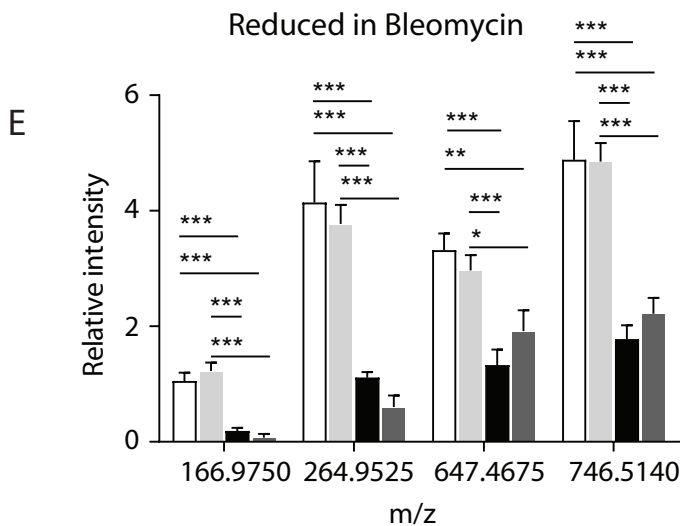
Reduced in Bleomycin



Enhanced in Bleomycin



Reduced in Bleomycin



Enhanced in Bleomycin

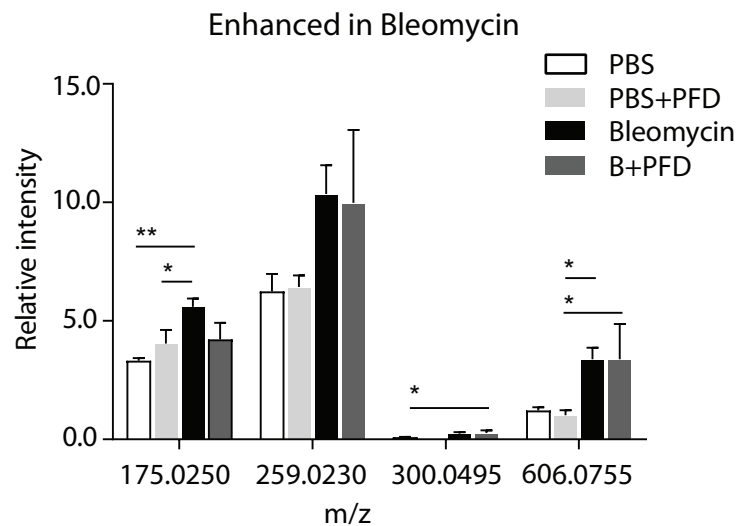


Figure 4

PBS
 PBS+PFD
 Bleomycin
 B+PFD

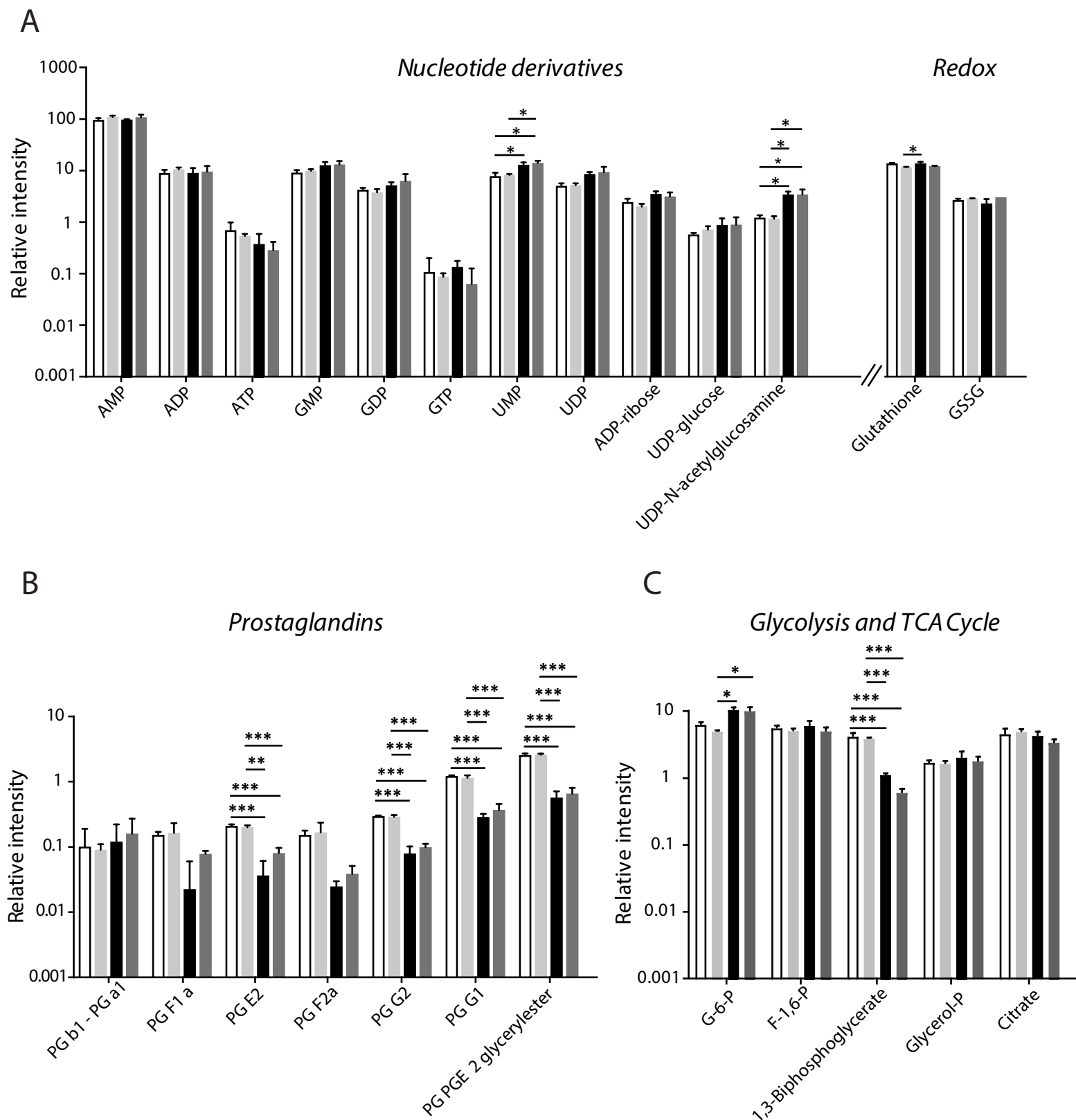


Figure 5

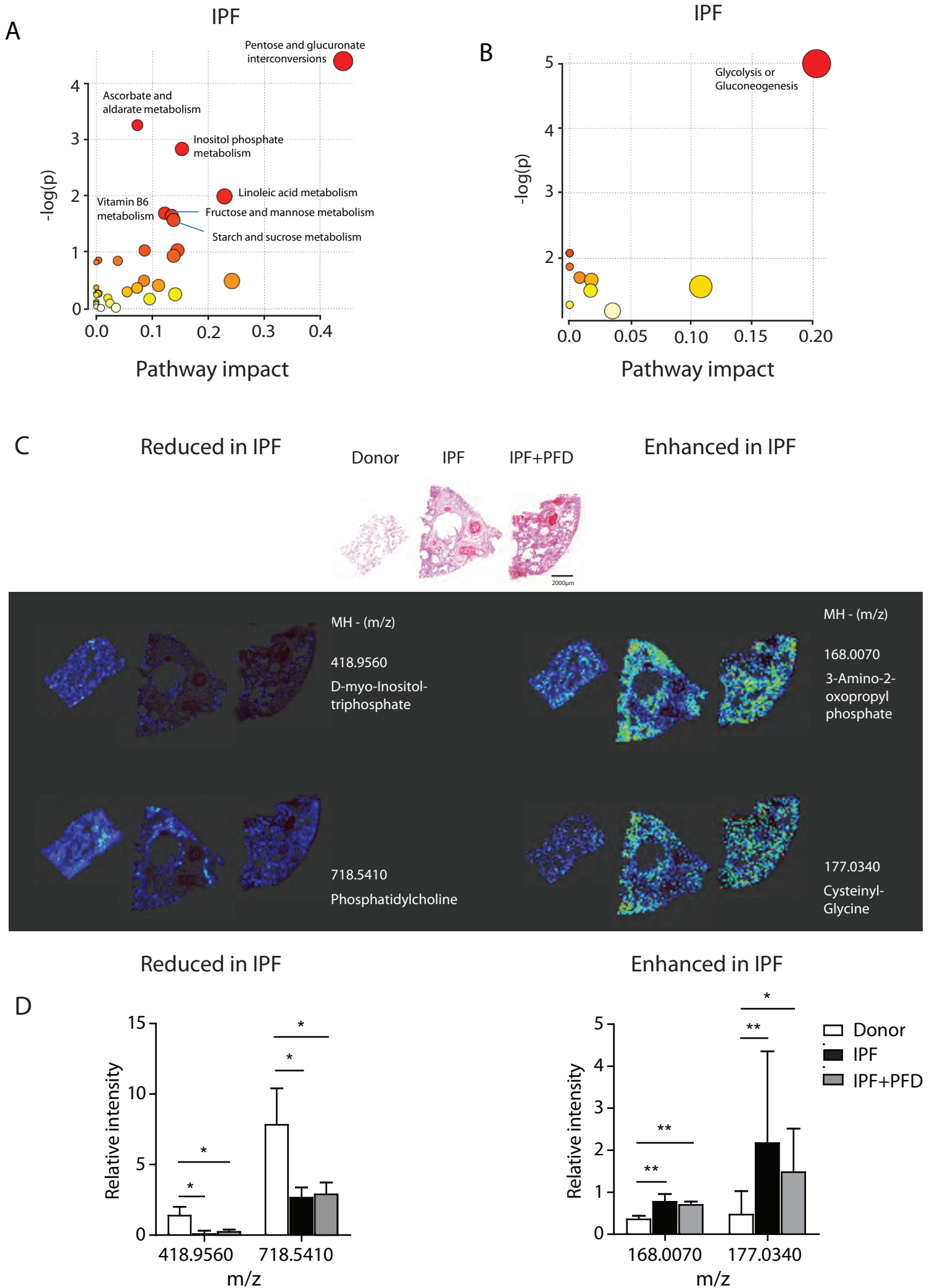
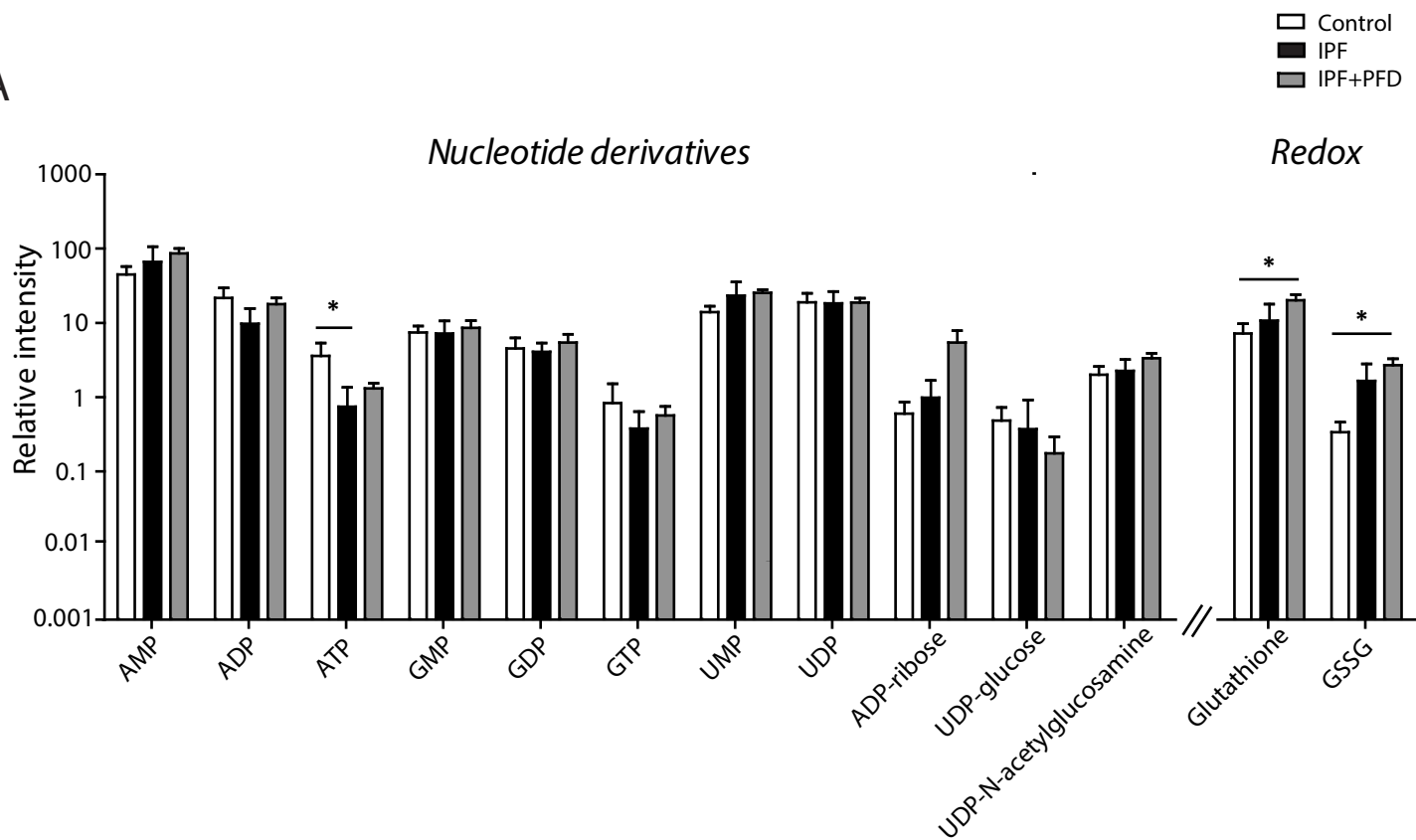
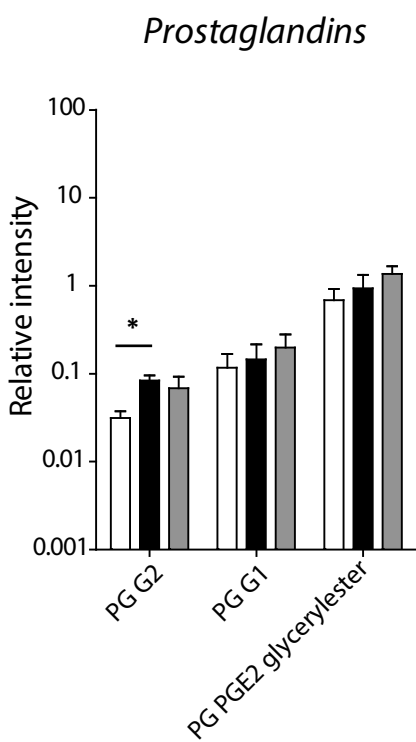


Figure 6

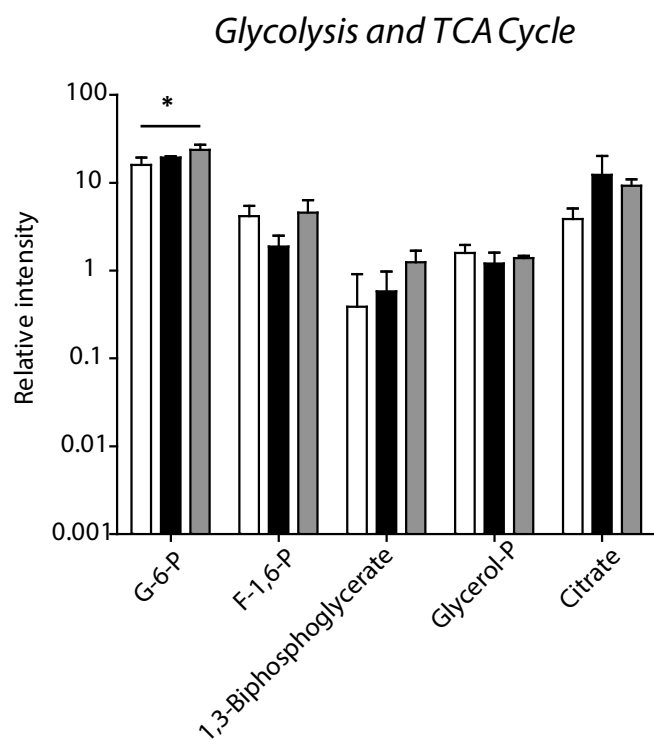
A



B



C



Supplementary information

Bleomycin-induced mouse model of pulmonary fibrosis and pirfenidone treatment

For this study, 8- to 10-week-old female C57BL/6N mice (Charles River Laboratories) were used for the experiments, which were performed in accordance with the recommendations in the Guide for the Care and Use of Laboratory Animals of the National Institutes of Health. Pulmonary fibrosis in mice was established as previously described (1). Briefly, bleomycin (3 U/kg) was dissolved in sterile phosphate-buffered saline (PBS) and applied intratracheally as a single dose to C57BL/6N mice. Control mice were given PBS. From day 7 to day 14, experimental animals were administered pirfenidone (Selleckchem, Houston, TX, USA) in carboxymethyl cellulose (CMC) by oral gavage daily. We used a dose of 500 mg/kg body weight pirfenidone, based on literature reports (2, 3). Control mice received CMC only. All animals (control=3, bleomycin=3, pirfenidone treatment=3) were sacrificed on day 14. The lungs were rapidly dissected, fresh-frozen in liquid nitrogen, and stored at -80°C until sectioned.

MADLI-MSI tissue preparation

The frozen tissues were cut into 12- μ m thick sections at -20°C using a microtome (Leica CM1950, Leica Microsystems, Germany). The sections were thaw-mounted onto indium tin oxide -coated MALDI target slides (Bruker Daltonics, Bremen, Germany) and stored at -80°C until further analysis.

For endogenous metabolite MALDI-MSI, the matrix solution was prepared by dissolving 9-aminoacridine hydrochloride monohydrate matrix (Sigma-Aldrich, Germany) in 70% methanol to a final concentration of 10 mg/ml. The matrix solution was sprayed by a SunCollect™ automatic sprayer (Sunchrom, Friedrichsdorf, Germany). The flow rate was 10, 20, 30, and 40 μ l/min for the first four layers, respectively. The next four layers were sprayed at 40 μ l/min. For MALDI-MSI of pirfenidone and the related metabolites 5-hydroxymethyl pirfenidone and 5-carboxy pirfenidone, a 30 mg/ml super-DHB matrix (Sigma-Aldrich) in 50% methanol containing 0.2% trifluoroacetic acid was applied using an automated spray coating machine, ImagePrep (Bruker Daltonics). Following the MALDI imaging experiments, the matrix was removed by washing with 70% ethanol. Then, slides were quickly dipped in

distilled water and stained with H&E. Slides were scanned with a MIRAX DESK digital slide-scanning system (Carl Zeiss MicroImaging, Göttingen, Germany).

Data processing and statistical analysis

Data processing

The acquired MSI data underwent spectra processing with FlexImaging v. 4.0 software (Bruker Daltonics). The raw data were normalized against the root mean square of all data points. The average spectra of defined regions of interest were exported as .csv files and subsequently processed by MATLAB R2013a (Mathworks, Natick, MA, USA). A self-implemented MATLAB analysis pipeline was performed as previously described (4), (5), (6). Basically, baseline correction was performed by interpolating between given equally spaced intervals (spacing 0.02 Da). Resampling was performed using a 0.005-Da step width, and the smoothing operation was carried out using a size 3 Kaiser-Window. Using an adapted version of the LIMPIC algorithm (7), peaks were picked using a minimal peak width of 0.0005, a noise-threshold of 2, and an intensity threshold percentage of 0.01. Isotopes were excluded. To identify statistically significant differences in m/z values, the peak lists were analysed using the Student's t -test (unpaired, two-tailed) and Benjamini-Hochberg *post hoc* test ($\alpha=0.05$). As a result, a list of significantly different metabolites could be achieved with a corresponding p -value of ≤ 0.05 and intensity fold-change of ≥ 1.5 .

Relative quantification of endogenous metabolites

The comparison of relative abundance of endogenous metabolites between different groups was performed using One-Way analysis of variance, with followed by Bonferroni test. Data is presented as bars or whiskers vertical graphs with mean \pm standard deviation.

Unsupervised hierarchical clustering

Hierarchical clustering was performed using the built-in FlexImaging v. 4.0 (Bruker Daltonics, Germany). Similar spectra are grouped using multivariate statistical analysis (8), (9). The created segmentation maps were used to identify areas in which similar spectra occur across the tissue sample. List of m/z species with respective intensities for selected regions were uploaded to MetaboAnalyst, processed with a mass tolerance of m/z 0.0001 and no

data filtering. Heatmap-based clustering was created with MetaboAnalyst (<http://www.metaboanalyst.ca>) (10).

Metabolite identification by LC-MS

The targeted metabolite identification by LC-MS was performed as described previously (5). Briefly, 30 mg of lung tissue was lysed with 1 ml cold 80% MeOH/20% water in NucleoSpinBeadTube (Macherey Nagel, Düren, Germany) for 3 min at a frequency of 30 Hz using a TissueLyser (Qiagen, Hilden, Germany). The supernatant was collected by centrifugation at $17,900 \times g$ at 4°C for 15 min. Then, 10 μl of tissue sample and 10 $\mu\text{g}/\text{ml}$ of single metabolite standards were injected into an XBridge Amide column (100 mm \times 4.6 mm ID, 3.5 μm ; Waters, Eschborn, Germany) via full-loop injection. LC-MS was performed on a Waters Acquity UPLC (Waters) coupled to maXis UHR-TOF-MS (Bruker Daltonics) using an established protocol (11). For confirmation of metabolite identity, the resulting mass spectra were compared against reference spectra from the measured standards.

References

1. Fernandez IE, Amarie OV, Mutze K, Konigshoff M, Yildirim AO, Eickelberg O. Systematic phenotyping and correlation of biomarkers with lung function and histology in lung fibrosis. *American journal of physiology Lung cellular and molecular physiology* 2016; 310: L919-927.
2. Schaefer CJ, Ruhmundt DW, Pan L, Seiwert SD, Kossen K. Antifibrotic activities of pirfenidone in animal models. *European respiratory review : an official journal of the European Respiratory Society* 2011; 20: 85-97.
3. Sun N, Fernandez IE, Wei M, Wu Y, Aichler M, Eickelberg O, A. W. Pharmacokinetic and pharmacometabolomic study of pirfenidone in normal mice tissues using high mass resolution MALDI-FTICR-mass spectrometry imaging. *Histochemistry and cell biology* 2015.
4. Aichler M, Borgmann D, Krumsiek J, Buck A, MacDonald PE, Fox JEM, Lyon J, Light PE, Keipert S, Jastroch M, Feuchtinger A, Mueller NS, Sun N, Palmer A, Alexandrov T, Hrabe de Angelis M, Neschen S, Tschop MH, Walch A. N-acyl Taurines and Acylcarnitines Cause an Imbalance in Insulin Synthesis and Secretion Provoking beta Cell Dysfunction in Type 2 Diabetes. *Cell metabolism* 2017; 25: 1334-1347 e1334.
5. Sun N, Ly A, Meding S, Witting M, Hauck SM, Ueffing M, Schmitt-Kopplin P, Aichler M, Walch A. High-resolution metabolite imaging of light and dark treated retina using MALDI-FTICR mass spectrometry. *Proteomics* 2014; 14: 913-923.
6. Buck A, Ly A, Balluff B, Sun N, Gorzolka K, Feuchtinger A, Janssen KP, Kuppen PJ, van de Velde CJ, Weirich G, Erlmeier F, Langer R, Aubele M, Zitzelsberger H, Aichler M, Walch A. High-resolution MALDI-FT-ICR MS Imaging for the analysis of metabolites from formalin-fixed paraffin-embedded clinical tissue samples. *The Journal of pathology* 2015.
7. Mantini D, Petrucci F, Pieragostino D, Del Boccio P, Di Nicola M, Di Ilio C, Federici G, Sacchetta P, Comani S, Urbani A. LIMPIC: a computational method for the separation of protein MALDI-TOF-MS signals from noise. *BMC bioinformatics* 2007; 8: 101.
8. Alexandrov T, Becker M, Deininger SO, Ernst G, Wehder L, Grasmair M, von Eggeling F, Thiele H, Maass P. Spatial segmentation of imaging mass spectrometry data with edge-preserving image denoising and clustering. *Journal of proteome research* 2010; 9: 6535-6546.
9. Alexandrov T, Becker M, Guntinas-Lichius O, Ernst G, von Eggeling F. MALDI-imaging segmentation is a powerful tool for spatial functional proteomic analysis of human larynx carcinoma. *Journal of cancer research and clinical oncology* 2013; 139: 85-95.
10. Xia J, Wishart DS. MetPA: a web-based metabolomics tool for pathway analysis and visualization. *Bioinformatics* 2010; 26: 2342-2344.
11. Yuan M, Breitkopf SB, Yang X, Asara JM. A positive/negative ion-switching, targeted mass spectrometry-based metabolomics platform for bodily fluids, cells, and fresh and fixed tissue. *Nature protocols* 2012; 7: 872-881.

Supplemental table 1. Patient characteristics

Supplementary figure 1. Clustering analysis and PLS-DA analysis

Supplementary figure 2. LC-MS data for metabolite identification.

Supplementary figure 3. On tissue MS/MS data for metabolite identification.

Supplementary table 2. Enriched pathway components of bleomycine induced pulmonary fibrosis in mouse.

Supplementary table 3. Enriched pathway components of human IPF samples.

Donor							
Age	53	29	60	37			
Gender	M	M	M	F			
Reason of rejection	Recipient dying	Contusion	Beginning fibrosis	Emboli			
Smoking	No but alcohol abuse/cirrhosis	No but drugs and alcohol	NA	No but IV drugs and alcohol			
NHBD	0	1	0	0			
Cause of death	CVA	Subdural hematoma	CVA	CVA			
PO2	468	360	386	407			
IPF	Untreated				Pirfenidone treated		
N							
Gender	M	M	M	M	M	M	M
Age at transplant	65	55	62	60	64	51	51
Height (cm)	168	168	162	167	176	172	177
Weight	65	73	52	72	75	81	77
Pirfenidone (2403mg/day) starting date	N.A.	N.A.	N.A.	N.A.	30.04.2013	26.03.2013	11.06.2013
Time of transplant	06.07.2010	26.06.2012	11.11.2012	02.05.2013	23.08.2013	30.09.2013	04.07.2014
Time of diagnosis	01.10.2009	01.12.2009	01.01.2011	01.07.2012	18.12.2012	01.11.2012	11.02.2013
Smoking history (current/ex/non)	ex						
PY	20	30	30	38	20	10	36
PFT							
FEV ₁ (%pred)	41	66	78	81	67	49	48
FEV ₁ (L)	1.16	2.08	1.98	2.61	2.18	1.64	1.74
FVC (%pred)	34	61	67	100	62	44	51
FVC (L)	1.26	2.38	2.12	3.71	2.58	1.88	2.3
TLC (%pred)	34	54	70	89	48	37	54
TLC (L)	1.31	3.45	3.91	5.56	3.48	2.5	3.92
DLco (%pred)	23	22	33	30	39	30	28
DLco (L)	1.9	1.97	2.44	NA	3.68	2.2	2.9

Supplementary table 1: Enriched pathway components of bleomycine induced pulmonary fibrosis in mouse. Significantly different metabolites (Student's t-test (unpaired, two-tailed) p-value ≤ 0.05 , intensity fold-change ≥ 1.5) of corresponding pathways are listed.

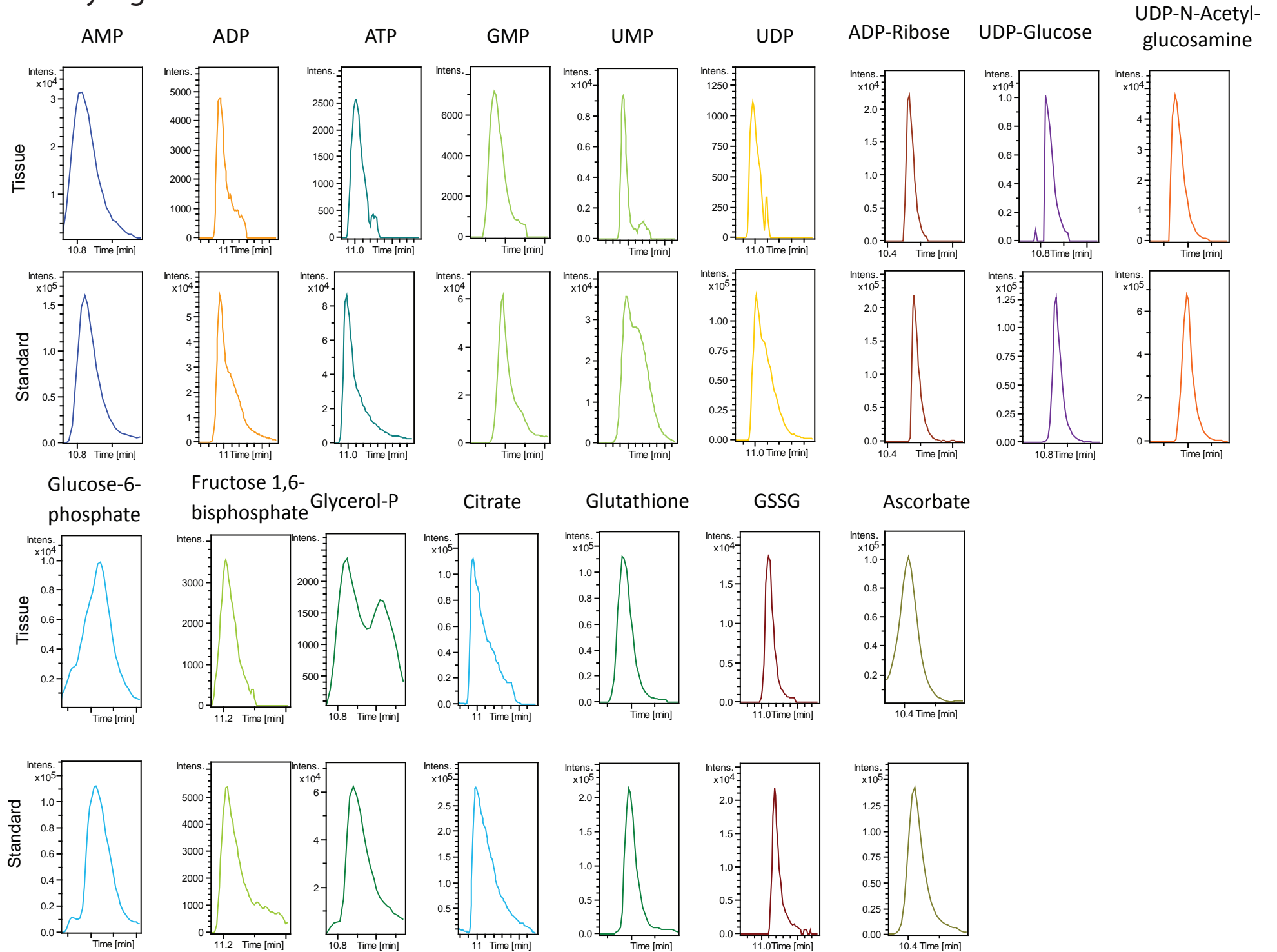
Fibrosis vs. Control	
Reduced in fibrosis	
Pathways	Metabolites
Glycolysis / Gluconeogenesis	Phosphoenolpyruvate
	3-Phospho-D-glycerate
	3-Phospho-D-glyceroyl phosphate
	2-Phospho-D-glycerate
	2,3-Bisphospho-D-glycerate
Enhanced in fibrosis	
Pathways	Metabolites
Amino sugar and nucleotide sugar metabolism	UDP-N-acetyl-alpha-D-glucosamine
	D-Glucose 1-phosphate
	UDP-glucuronate
	UDP-N-acetyl-D-galactosamine
	D-Mannose 6-phosphate
	N-Acetyl-D-glucosamine 6-phosphate
	UDP-D-galacturonate
	D-Mannose 1-phosphate
	UDP-N-acetyl-D-mannosamine
	UDP-L-iduronate
	beta-L-Arabinose 1-phosphate
	N-Acetyl-D-mannosamine 6-phosphate
	N-Acetyl-alpha-D-glucosamine 1-phosphate
Pentose and glucuronate interconversions	D-Glucose 1-phosphate
	UDP-glucuronate
	D-Ribulose 5-phosphate
	D-Xylulose 5-phosphate
	D-Mannonate
	L-Gulonate
	D-Altronate
	L-Ribulose 5-phosphate
	5-Dehydro-4-deoxy-D-glucuronate
	(4S)-4,6-Dihydroxy-2,5-dioxohexanoate
	L-Xylulose 1-phosphate
L-Galactonate	
Ascorbate and aldarate metabolism	Ascorbate
	UDP-glucuronate
	D-Xylulose 5-phosphate
	L-Gulonate
	L-Ribulose 5-phosphate
	D-Glucuronolactone
	L-xylulose-Hexulonolactone
	beta-L-Galactose 1-phosphate
	L-Galactonate
L-Ascorbate 6-phosphate	
Pentose phosphate pathway	D-Ribose 5-phosphate
	D-Ribulose 5-phosphate
	D-Xylulose 5-phosphate
	D-Gluconic acid
	alpha-D-Ribose 1-phosphate
	beta-D-Glucose 6-phosphate

	D-arabino-Hex-3-ulose 6-phosphate
Fructose and mannose metabolism	D-Mannose 6-phosphate
	D-Mannose 1-phosphate
	D-Fructose 1-phosphate
	Sorbose 1-phosphate
	beta-D-Fructose 2-phosphate
Pirfenidone treatment vs. non-treated fibrosis	
Reduced after pirfenidone treatment	
Pathways	Metabolites
Ascorbate and aldarate metabolism	Ascorbate
	Monodehydroascorbate
	D-Glucuronolactone
	L-xylo-Hexulonolactone

Supplementary table 2: Enriched pathway components of human IPF samples. Significantly different metabolites (Student's t-test (unpaired, two-tailed) p-value ≤ 0.05 , intensity fold-change ≥ 1.5) of corresponding pathways are listed.

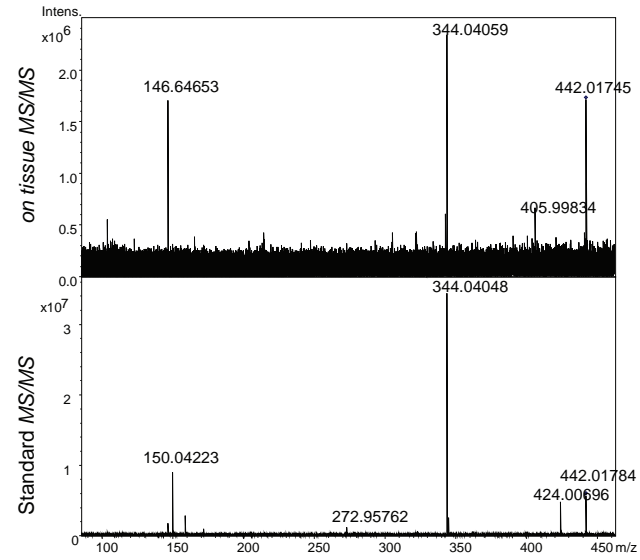
Human IPF vs. normal	
Reduced in human IPF	
Pathways	Metabolites
Linoleic acid metabolism	Phosphatidylcholine
	13(S)-HODE
	9(S)-HODE
	9(10)-EpOME
	12(13)-EpOME
Inositol phosphate metabolism	1D-myo-Inositol 1,4-bisphosphate
	1D-myo-Inositol 1,3,4-trisphosphate
	D-myo-Inositol 1,4,5-trisphosphate
	D-myo-Inositol 1,3-bisphosphate
	D-myo-Inositol 3,4-bisphosphate
Starch and sucrose metabolism	UDP-glucuronate
	UDP-D-galacturonate
	alpha-D-Glucose 1,6-bisphosphate
Enhanced in human IPF	
Pathways	Metabolites
Pentose and glucuronate interconversions	D-Glucuronate
	D-Galacturonate
	D-Lyxose
	D-Mannonate
	D-Tagaturonate
	3-Dehydro-L-gulonate
	L-Gulonate
	D-Altronate
	D-Fructuronate
	L-Galactonate
Ascorbate and aldarate metabolism	D-Glucuronate
	D-Galacturonate
	3-Dehydro-L-gulonate
	L-Gulonate
	Dehydroascorbate
	L-Galactonate
Vitamin B6 metabolism	4-Pyridoxate
	2-(Hydroxymethyl)-3-(acetamidomethylene)succinate
	3-Hydroxy-4-hydroxymethyl-2-methylpyridine-5-carboxylate
	3-Amino-2-oxopropyl phosphate
Fructose and mannose metabolism	L-Fuculose 1-phosphate
	L-Rhamnulose 1-phosphate
	L-Fucose 1-phosphate
Pirfenidone treatment vs. non-treated IPF	
Enhanced after pirfenidone treatment	
Pathways	Metabolites
Glycolysis / Gluconeogenesis	3-Phospho-D-glycerate
	2-Phospho-D-glycerate

Supplementary Figure 1

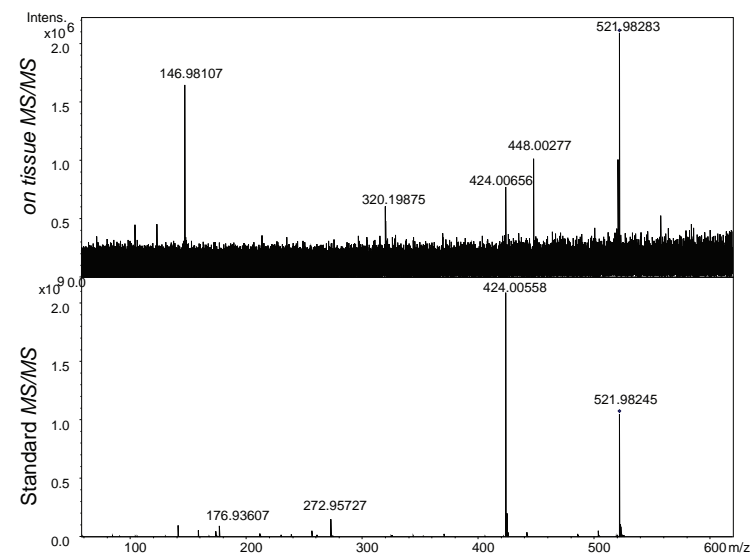


Supplementary Figure 2

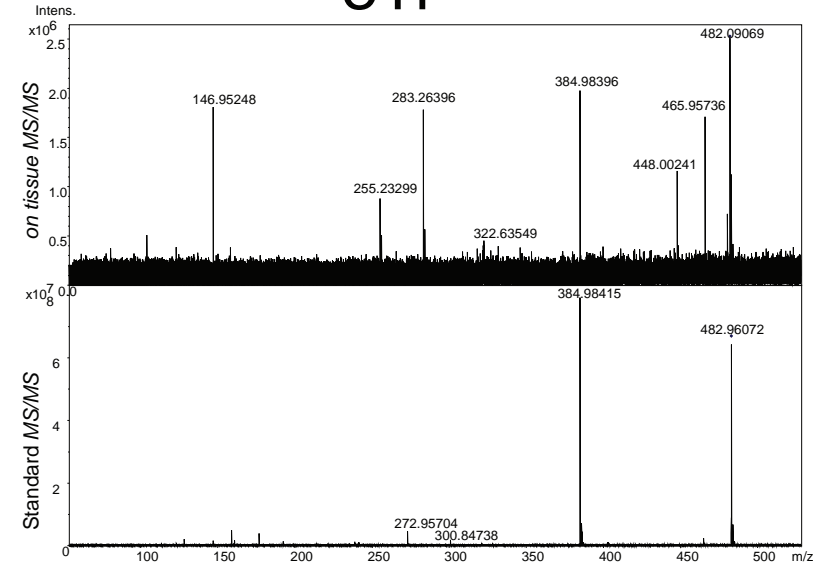
GDP



GTP

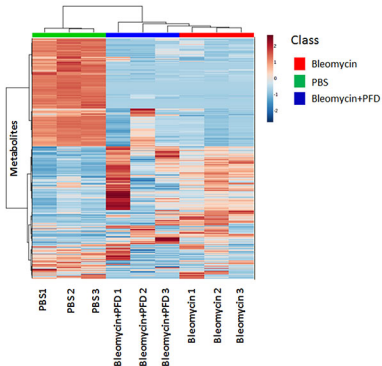


UTP



Clustering analysis

A



PLS-DA analysis

B

